Virus-host metabolic interactions: using metabolomics to probe oxidative stress, inflammation and systemic immunity

Schoeman, J.C.

Chapter 7

Increased *in utero* metabolic stress elicits pro-inflammatory immune responses in cART-exposed infants born to HIV-infected women

Johannes C. Schoeman, Gontse P. Moutloatse, Amy C. Harms, Rob J. Vreeken, Henriette J. Scherpbier, Liesbeth Van Leeuwen, Theo W. Kuijpers, Carools J. Reinecke, Ruud Berger, Thomas. Hankemeier, and Madeleine J Bunders

Submitted for publication

Abstract

Although combination antiretroviral therapy (cART) to HIV-infected women during pregnancy has dramatically reduced the risk of mother-to-child (MTCT) transmission of HIV, there are concerns regarding potential adverse effects on growth and immune development in the infants following *in utero* cART exposure. cART is known to alter lipid metabolism and mitochondrial function, and disturb cell homeostasis in HIV-infected patients. The activation of these metabolic stress signaling pathways can lead to an array of responses including activation of innate immune responses and restriction of (cell) growth. However, it is unknown whether *in utero* cART exposure of the fetus born to HIV-infected women leads to dysregulation of fetal metabolism with implications for growth and immunity. Using novel comprehensive targeted metabolomics analyses of cord blood plasma, we investigated the impact of *in utero* HIV and cART exposure on the infants' (n = 12) metabolome focusing on the lipid and mitochondrial compartment compared to HIV-unexposed uninfected infants (HUU) (n = 15). The lipid profile was significantly altered in cART and HIV-exposed uninfected (HEU) infants, with increased triglyceride and decreased phospholipid species compared to control infants without *in utero* HIV and cART exposure. Furthermore, we detected an increase in oxidized lipids, which are the main products of reactive oxygen species (ROS) generated by dysregulated mitochondria. Compensatory mechanisms for restoring homeostasis and reducing cell stress signaling (e.g., cytochrome p450 activity) were reduced in HEU children with *in utero* cART exposure compared to HUU infants. Finally, the alterations in lipid metabolites and lipid peroxidation products were associated with increased levels of pro-inflammatory lysophospholipids as well as the pro-inflammatory cytokines IL-1β and IP-10 respectively. Taken together, these data reveal disturbance of cell homeostasis following *in utero* cART and HIV exposure leading to increased immune activation in the infant.

Background

Combination antiretroviral therapy (cART) in HIV-infected pregnant women reduces the risk of mother-to-child (MTCT) transmission of HIV from 25-40% to less than 2% [1–3]. The global effort to provide cART for pregnant HIV-infected women has dramatically reduced the number of newly infected infants, while at the same time leading to the rapid increase of HIV-exposed, uninfected infants (HEU), which are exposed to long-term cART *in utero*. Although the HEU infants are presumed to be healthy, elevated morbidity and mortality is reported in these infants ranging from increased susceptibility to infections to neurological abnormalities [4–7]. The underlying mechanisms responsible for these observations remain largely unknown; however, there are suggestions that *in utero* cART exposure induces metabolic dysregulation with consequences for growth, development and immune competence. cART is known to alter lipid metabolism and mitochondrial functioning in HIV-infected patients, including pregnant HIV-infected women [8–14]. Altered acyl-carnitine profiles [15] and reduced mitochondrial DNA levels were reported in cART-exposed HEU infants compared to HIV-unexposed and uninfected (HUU) infants [5,16–18]; both of which are reflective of mitochondrial dysregulation.

Disruption of cell homeostasis by cART-induced alteration in mitochondrial functioning and lipid metabolism may be particularly relevant during fetal development, as the demand for nutrients and energy is high. Cell stress due to altered metabolite levels is sensed by and activates highly conserved nutrient-sensing (stress) receptors in the endoplasmic reticulum (ER) [19,20]. For example, excessive production of reactive oxygen species (ROS) due to mitochondrial dysfunction triggers the unfolded protein response (UPR) activating transcription factor 6 (ATF6) and inositol-requiring protein 1 (IRE1), which induce lipogenesis[21]. Furthermore, ER stress activates the unfolded protein responses (UPR's) pro-inflammatory c-Jun N-terminal kinase (JNK) and mitogen-activated protein kinase (MAPK) pathways [22,23]. In obese patients altered lipid levels leading to ER stress result in low-level inflammation observed as part of the metabolic syndrome [22,24]. Although, HEU infants are suggested to be more susceptible to infections, innate and adaptive arms of the immune system have been reported to exhibit a pro-inflammatory signature [25–28]. These altered immune responses have been attributed to maternal HIV infection; however, the underlying mechanism is unknown, as HIV is not present in the infant. As described above, metabolic processes are critical modulators of immune responses [29–34]. Therefore, we hypothesized that *in utero* cART exposure induces metabolic dysregulation, which shapes the immune response in the infant.

Recently developed metabolomics techniques provide the unique opportunity to characterize the complexity of the metabolome with high sensitivity. Given the rapidly increasing number of HEU infants who are exposed *in utero* to cART, information on potential adverse effects of this exposure is crucial. Here, we used targeted metabolomics to compare the metabolite profile in cord blood obtained from cART-exposed HEU infants with HUU control infants born to healthy women. To determine the interaction between metabolites and immune responses we quantified levels of classical cytokines and chemokines in the same cord blood sample. Together, these analyses provide a unique metabolite prolife to determine the impact of cART induced metabolic dysregulation of cell homeostasis and activation of pro-inflammatory immune responses.

Methods

Patients

Plasma was obtained from cord blood collected from 12 HEU infants that were exposed *in utero* to HIV and cART; plasma was also obtained from cord blood collected from 15 HUU infants who were born to HIV-negative mothers (and therefore not exposed to cART). The samples were collected at the Academic Medical Center (Amsterdam, the Netherlands). The study was approved by the local ethics committee and informed consent was obtained from participating mothers. For the HEU group, maternal viral load, $CD4^+$ T cell count, and antiretroviral medications were obtained from the patient hospital records (**Supplementary Table S7.1**). The cART regimen that was used for each patient (**Table S7.1)** was based on viral resistance or the patient's treatment regimen prior to conception. According to guidelines established by the World Health Organization, the cART regimen consisted of two NRTI's (primarily zidovudine and lamivudine) and either a protease inhibitor (ritonavir-boosted lopinavir or nelfinavir) or an NNRTI (nevirapine). One patient took tenofovir/emtracitibine during the first trimester of pregnancy only combined with lamivudine and nevirapine, while another received nevirapine (NNRTI), in combination with Kaletra and saquinavir due to her individual resistance profile. During birth, all HIV-infected mothers were given intrapartum zidovudine. The clinical profile at delivery of the 12 mothers in the study indicates that the virus was suppressed appropriately, consistent with a mother-to-child transmission rate of <1%. The HIV-1 status of the infants was determined according the national protocol in the Netherlands for prevention of MTCT of HIV. HIV infection was evaluated at birth, 5 weeks and three months by measuring RNA viral load with PCR. At 18 months of age, HIV status of the infants was confirmed by showing absence of detectable HIV IgG. All infants were confirmed HIV-negative.

Sample collection

Immediately following delivery, umbilical cord blood was obtained from the clamped umbilical cord. Samples were collected in chilled heparin-containing Vacutainer tubes, and the plasma was separated by centrifugation at 5000×*g* for 10 min at 4°C. Aliquots of plasma were stored at -80°C prior to analysis and transported to the Biomedical Facility Leiden (Leiden University) for metabolomics analysis.

Quality control samples

Quality control (QC) samples were used during the metabolomics analyses for quality assurance purposes. Equal volumes of each study sample were pooled to generate a QC pool. A set of QC samples was then included in the analyses with the experimental groups on the individual metabolomics platforms, and the QC samples were distributed randomly through the samples prior to liquid chromatography–mass spectrometry (LC-MS) analysis. In addition, independent duplicate samples were randomly selected when sample volume permitted (10-15% of samples). Using the QC samples and duplicate samples, a double-quality-control approach was used to include metabolites that were measured accurately by the individual metabolomics platforms; only those metabolites for which the duplicate and QC samples had a relative standard deviation <30%, were considered to be measured accurately.

LC-MS targeted metabolomics analyses

Targeted metabolomics analyses were performed using standard operating procedures based on previously published methods [35,36]. The detailed procedures and target lists are provided in the Supplementary Methods.

Positive and negative lipid profiling

10-µl and 20-µl serum samples were spiked with calibration and internal standards and extracted using isopropyl alcohol (for the positive lipid platforms) or methanol (for the negative lipid platforms). Samples were analyzed using an ACQUITY UPLC system coupled to a 6530 Accurate Mass QToF (Agilent Technologies, Santa Clara, CA) [36].

Oxylipin profiling

150-µl serum samples were spiked with calibration and internal standards and diluted with a 5% methanol solution containing 0.1% acetic acid. Samples were extracted using solid-phase extraction (HLB Oasis, Waters Chromatography) and analyzed using an HPLC system coupled to a 6460 Agilent Triple Quadrupole mass spectrometer (Agilent Technologies) [35].

Soluble immunological factors

A multiparameter Luminex bead assay (Invitrogen) was used to measure the levels of the following soluble factors in accordance with the manufacturer's instructions: IL1-β, IL-4, IL-5, IL-6, IL-8, IL-10, IL-13, IL-17A, IL-18, IFN-α, IFN-γ, IP-10, TNF-α, MIP-1α, MIP-1β, RANTES, and GM-CSF. Human serum CRP was measured with ELISA (R&D systems, Abingdon, United Kingdom).

Statistical data analyses

A combination of univariate bioinformatics approaches was performed using the R script–based online tool Metaboanalyst 3.0, a comprehensive tool suitable for analyzing metabolomics data [37]. Mann-Whitney U-test, and Fisher's exact test were used to compare differences in patient demographics on continues and categorical variables respectively using SPSS version 23.0 (IBM Corp., Armonk, NY). Pearson's correlation coefficients were calculated using SPSS. Significant Pearson correlations between immunological markers and metabolites were visualized using the Metscape application within Cytoscape (v3.2.1) [38].

Following LC-MS analysis, peak integration, and determination of the relative ratios between metabolites and their corresponding internal standards, quality assurance was performed using the QC and duplicate samples. First, we evaluated the quality of the samples and assessed outliers based on a 95% confidence region in a Hotelling's T-squared distribution test. In all of the platforms measured, homogeneity was found among the two separate groups, and none of the samples were identified as outliers. Significant metabolites were identified based on the following two criteria: *i*) a fold change (FC) ≥1.25 or ≤0.75, indicating a 25%

increase or decrease, respectively, and *ii*) a *p*-value <0.05 using the Mann-Whitney *U* test. The significant univariate results are shown on a volcano plot as colored symbols. Pearson's correlation coefficients were generated using log-transformed normalized data in SPSS. During the correlation analyses, each metabolite was tested against eight immunological markers, and no multiple testing correction was performed. Significant correlations were defined as a Pearson's coefficient (*r*) >0.46 or *r* <-0.46 and $p<0.05$.

Results

Patient demographics

In this prospective study, 12 HIV-infected - and 15 HIV-negative pregnant women were included. The baseline maternal group demographics (**Table 7.1**) were similar with regards to age, maternal pre-pregnancy BMI, and the gestation. More HIV-infected mothers were black compared to the mothers included in the control group ($p = 0.03$). As clinical metabolic measurements are not part of standard pregnancy care, these were only available for the HIV-infected women. Both triglycerides (1.8 mmol/L) and total cholesterol (5 mmol/L) were within upper-normal ranges for pregnant women [39] . None of the women in both groups suffered from gestational diabetes. The HIV-infected women were in a good clinical condition and had a $CD4^+$ T cell count in the first-trimester exceeding $200x10^6$ cell/L (**Table 7.1**). After initiating cART, the $CD4^+$ T cell counts increased and viral load decreased; at delivery, viral load was undetectable in all women (**Table 7.1)**. All mothers received cART in accordance with EACS guidelines including at least two nucleotide reverse transcriptase inhibitors (NRTIs) in combination with either a protease inhibitor (PI) or non-nucleotide reverse transcriptase inhibitor (NNRTI). Most women received zidovudine, lamivudine and ritonavir boosted lopinavir (n=8) (Table S1). None of the HIV-infected mothers transmitted the virus to their infant, which was verified via follow-up testing. The HEU and HUU infants were similar with regards to gestational age, birth weight, 1 and 5 min apgar scores, mode of delivery and gender. Only two infants, one in the HEU and one in the HUU, were small for gestational age (SGA).

Mitochondrial dysfunction and oxidative stress in cART-exposed HEU infants

To assess mitochondrial functioning, we measured ROS-catalyzed lipid peroxidation metabolites (oxylipins) [40–43]. Using predefined criteria to identify significantly altered metabolites using the Mann-Whitney *U* test and Fold Change (FC) measurements (see Methods), 13 ROS-produced oxylipins were identified to be significantly increased in the cART-exposed HEU infants compared to controls. None of the oxylipins were decreased in the cART-exposed HEU infants (**Fig. 7.1** and **Table S7.2**). One infant was not exposed *in utero* to NRTI's and had lipid peroxidation metabolite profile comparable to those of the HUU infants. These findings indicate that compared to control infants, cART-exposed HEU infants have significantly altered mitochondrial functioning resulting in increased ROS production. As ROS are strong activators of lipogenesis, we next investigated whether *in utero* exposure to cART caused changes in the infants' lipid profiles.

Table 7.1: Patient Demographics

Clinical variables		Control mother (n = 15) & HUU infants (n = 15)	HIV positive mother (n = 12) & HEU infants (n = 12)	
		Median (75% CI)	Median (75% CI)	*p-value*
Mothers				
Age (years)		32.6 (30.7 - 33.2)	28.5 (28.2 -32.4)	0.50[a]
Pre-pregnancy weight (kg)		64.5* (62.7 - 66.9)	68.5 (65.7 - 74.2)	0.41[a]
Pre-pregnancy BMI		22.04* (22.3 - 24.1)	23.67 (22.6 - 26.1)	0.79[a]
Total Triglycerides# (mmol/L)		-	1.80** (1.5 - 2.1)	
Total Cholesterol# (mmol/L)		-	5 ** (4.6 - 5.4)	
Glucose# (mmol/L)		-	4.30** (4.2 - 4.7)	
Ethnicity (W/B/SA)		9/4/2	3/9/0	0.03[b]
Gestational Diabetes (Yes/No)		0/15	0/12	
HIV viral load (copies/mL)	**1st trimester**	-	528.5 (1269 - 9084)	
	2nd trimester	-	50 (47.81 - 281)	
	3rd trimester	-	0	
CD4 count (10E6 cells/L)	**1st trimester**	-	455 (465.5 - 594.5)	
	2nd trimester	-	520 (511.4 - 650.6)	
	3rd trimester	-	700 (616.5 - 792.5)	
Infants				
Gestation period (weeks)		40 (37.63 - 39.97)	39.25 (38.74 - 39.82)	0.57[a]
Birth weight (g)		3380 (3128 - 3494)	3085 (3009 - 3472)	0.34[a]
Apgar scores	**1 min**	9 (8.6 - 9.2)	9 (7.4 - 9.1)	0.91[a]
	5 min	10 (9.5 - 9.9)	10 (9.1 - 9.9)	0.44[a]
Mode of delivery (Vag/CS)		14/1	8/4	0.14[b]
Gender (Male / Female)		8/7	7/5	0.55[b]

[a] Mann-Whitney U-test; [b] Fisher's exact test; # Measured at the end of the 2nd trimester; *(**) 1(2) missing value(s)

W - White; B - Black; SA - South Asian; Vag - Vaginal; CS - Caesarean section; CI – Confidence interval

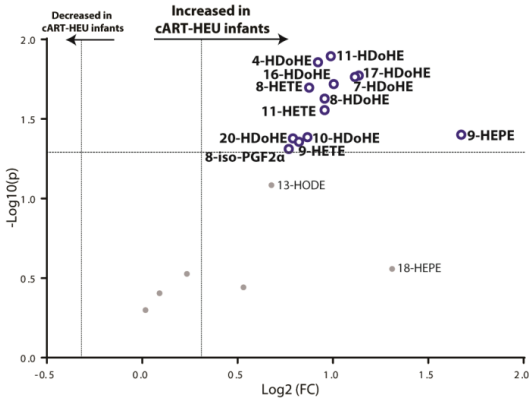

Figure 7.1: Volcano plot of the ROS-produced oxylipin profiles. Thirteen metabolites were identified as significantly increased (blue circles) in the cART-exposed HEU infants compared to HUU infants. HDoHE, hydroxyl-docosahexaenoic acid; HETE, hydroxy-eicosatetraenoic acid; HEPE, hydroxy-eicosapentaenoic acid; 8-iso-$PGF_{2\alpha}$, 8-iso-prostaglandin $F_{2\alpha}$.

Lipid profiles in cART-exposed HEU infants are characterized by hypertriglyceridemia

We evaluated the effect of *in utero* cART-HIV exposure on lipid metabolism in infants by measuring triglyceride, diacylglycerol, sphingomyelin, cholesterol ester, and free fatty acid profiles. We found that triglycerides with long and very long acyl chains were significantly increased in cART-exposed HEU infants compared to HUU control infants, suggesting that non-specific fatty acid elongation and biosynthesis were increased. In total, 2 diacylglycerols and 32 triglycerides were increased in the cART-exposed HEU infants compared to HUU control infants (**Fig. 7.2** and **Table S7.2)**. In contrast, we observed no significant difference between cART-exposed HEU infants and HUU infants with respect to free fatty acids, cholesteryl esters, or sphingomyelin levels (**Fig. 7.2**).

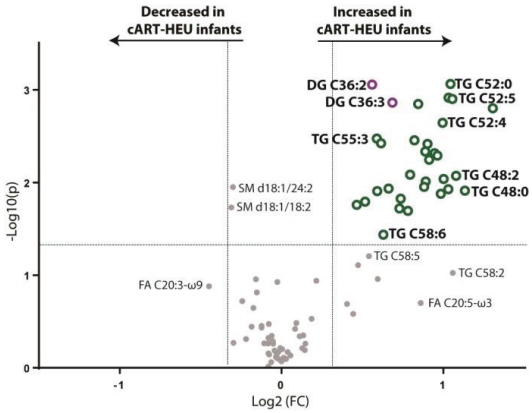

Figure 7.2: Volcano plot of lipid profiles. The 32 triglycerides and 2 diacylglycerols that were increased in cART-exposed HEU infants compared to HUU infants are shown as green and purple circles, respectively. TG, triglyceride; SM, sphingomyelin; CE, cholesteryl ester; FA, free fatty acid.

Hypertriglyceridemia is commonly observed in cART-treated HIV-infected adults. In particular, lopinavir, to which 8 of 12 infants were exposed to, increases triglyceride levels and to a lesser extend the NRTIs stavudine and abacavir[44–48].The slightly elevated triglyceride levels in cART-treated HIV-infected pregnant women cannot directly account for the increased levels of triglycerides measured in the infant, as only free fatty acids are transported across the placenta to the fetus [49], and no differences in free fatty acids between cART-exposed HEU infants and HUU infants were detected. Increased triglyceride levels in the infant depend on endogenous triglyceride synthesis, which occurs primarily on the ER. When triglycerides levels are high, triglycerides accumulate within the ER intermembrane space. To remove the surplus of triglycerides from the ER, the ER commences the formation of lipid droplets with an outer rim of ER membrane–derived phospholipids. Depletion of ER membrane-derived phospholipids serves as an ER stressor[50].

Decreased phospholipids in cART-exposed HEU infants

We therefore evaluated phosphatidylcholines and phosphatidylethanolamines, which are the most prevalent glycerophospholipids and components of the ER membrane. Our analysis revealed significant changes in glycerophospholipid levels (**Fig. 7.3**). Specifically, three phosphatidylcholines (C32:0, C32:1, and C36:3), two plasmalogen phosphatidylcholines (C34:1 and C36:4), and one phosphatidylethanolamine (C38:4) were significantly decreased in cART-exposed HEU infants compared to HUU infants (**Fig. 7.3, Table S7.2**).

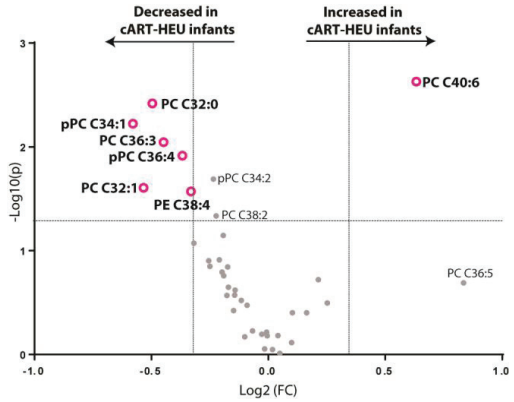

Figure 7. 3: Volcano plot of glycerophospholipid profiles. Overall, glycerophospholipids were reduced in the cART-exposed HEU infants compared to HUU infants. The glycerophospholipids, which were significantly altered are shown as pink circles. PC, phosphatidylcholine; pPC, plasmalogen phosphatidylcholine; PE, phosphatidylethanolamine.

Overall, we observed a decrease in phospholipid species in the cART-exposed HEU infants compared to control infants. In addition to their role in ER homeostasis, phospholipides - and specifically the hydrolysis products of phosphatidylcholines such as unsaturated lysophospholipids - have anti-inflammatory properties, inhibiting NF-κB activation via the MAPK pathway [51,52] while saturated lysophospholipds have a pro-inflammatory effect. As alterations in the lipid metabolism by cART-exposure may impact immune modulation by these metabolites, we subsequently assessed the lysophospholipid in both cART-exposed HEU infants and HUU infants.

CART-exposed HEU infants have increased levels of pro-inflammatory lysophospholipids

Two saturated stearic acid isomers (SN_1-lysophosphatidylcholine C18:0 and SN_2-lysophosphatidylcholine C18:0) and two saturated lysophosphatidylethanolamine species (C16:0 and C18:0) were significantly increased in cART-exposed HEU infants compared to HUU infants (**Fig. 7.4**, **Table S7.2**). Saturated lysophosphatidylcholines are robust pro-inflammatory molecules that activate cellular pathways, resulting in the production of IL-1β, IL-6, and IL-8, as well as arachidonic acid secretion [53–56]. The functions of saturated lysophosphatidylethanolamines are less understood, although these molecules are structurally quite similar to saturated lysophosphatidylcholines. The unsaturated ω-9 SN_1-lysophosphatidylcholine C20:3 was reduced compared to HUU infants [55].

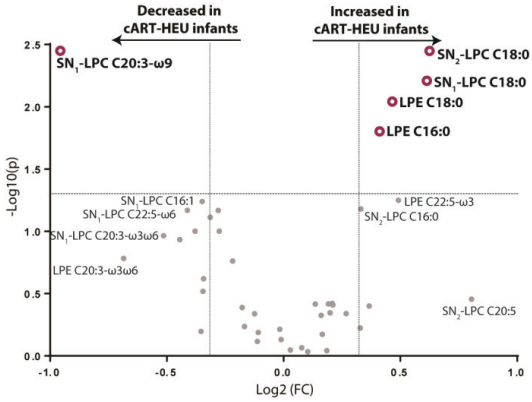

Figure 7.4: Volcano plot of lysophospholipid profiles. The increased saturated lysophospholipids and decreased unsaturated lysophospholipid in the cART-exposed HEU infants are shown as maroon symbols. LPC, lysophosphatidylcholine; LPE, lysophosphatidylethanolamine.

The analyzes of the ratio of saturated versus unsaturated lysophosphatidylcholines and lysophosphatidylethanolamines revealed that saturated species were twice as abundant as unsaturated species in the cART-exposed HEU infants (**Fig. S7.1**). In contrast, this ratio was balanced in the control group, indicating that unexposed infants maintain homeostatic control.

Compensatory anti-inflammatory oxylipin mediators are decreased in cART-exposed HEU infants impairing homeostatic control

Similar to lysophospholipids, the precursors of enzymatically synthesized oxylipins are produced by enzyme-mediated hydrolysis of membrane phospholipids, providing further assessment of the balance between pro-inflammatory and anti-inflammatory lipid mediators. This analysis revealed eight metabolites in the cyclooxygenase (COX), lipoxygenase (LOX), and cytochrome P450 (CYP) pathways that differed significantly between cART-exposed HEU infants and HUU infants (**Fig. 7.5** and **Table S7.2**). Specifically, the CYP oxylipins 5,6-DiHETre, 8,9-DiHETre, and 11,12-DiHETre were significantly reduced in the cART-exposed HEU infants, indicating impaired CYP metabolism in this group. DiHETrEs eicosanoids are the stable, inactivated form of the short-lived active signaling mediators epoxyeicosatrienoic acids (EETs). Interestingly, 11,12-EET—which was significantly reduced in cART-exposed HEU infants compared to HUU infants—is a potent inhibitor of the NF-κB pathway [57,58]. EETs also affect mitochondrial functioning and lipid metabolism by activating PPARα, which in turn induces mitochondrial β-oxidation. Furthermore, EETs regulate the secretion of insulin and glucagon via PPARα, thereby acting as anti-hyperlipidemia and anti-hyperglycemia agents [59,60]. The reduction in DiHETrE levels indicates reduced anti-hyperlipidemia capacity and increased ER stress in cART-exposed HEU infants.

The other four identified enzyme-derived oxylipin metabolites are in the LOX pathway and included 20-carboxy-LTB_4, protectin DX (PDX), 5-HEPE, and 9-HOTrE. Notably, 20-carboxy-LTB_4, which was increased in the cART-exposed HEU infants, is the stable downstream metabolite of leukotriene B_4, a potent pro-inflammatory mediator in asthma [61,62]. Overall, the changes in oxylipin levels measured in cART-exposed HEU infants indicate that the immune system in these infants is predisposed to develop pro-inflammatory responses, while compensatory mechanisms to reduce hyperlipidemia are reduced.

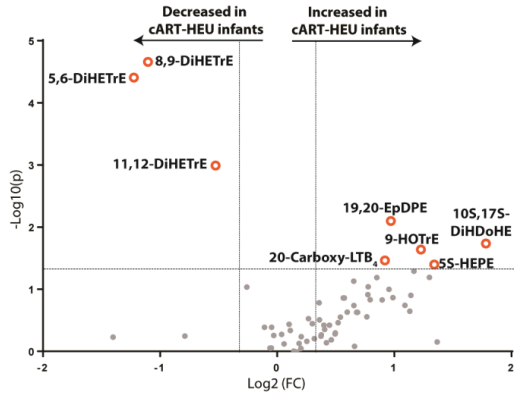

Figure 7.5: Volcano plot of COX, LOX, and CYP oxylipin profiles. Significantly increased or decreased oxylipins in the cART-exposed HEU infants compared to the HUU infants are shown as orange circles. DiHETrE, dihydroxy-eicosatrienoic acid; EpDPE, epoxy-docosapentaenoic acid; DiHDoHE, dihydroxydocosa-4,7,11,13,15,19-hexaenoic acid; HOTrE, hydroxy-9Z,11E,15Z-octadecatrienoic acid; HEPE, hydroxy-eicosapentaenoic acid; 20-carboxy-LTB_4, 20-carboxy-leukotriene B_4.

Increased levels of pro-inflammatory cytokines and chemokines correlate to specific metabolites derived from lipid metabolism and mitochondria in cART-exposed HEU infants

We aimed to confirm the proinflammatory milieu based on the above described oxylipin profile, by examining in addition classically measured cytokines and chemokines unsing a multiplex bead assay and assess a correlation between the metabolites and hallmark immune markers of inflammation in cART-exposed HEU and HUU infants [27]. **Fig. 7.6** shows correlation networks for the metabolite classes that correlated significantly to the immunological markers (**Tables S7.3-S7.7**); multiple testing correction was not performed, as only class responses—and not individual correlations—were interpreted. Overall, we found that triglycerides, diacylglycerols, and phospholipids (**Fig. 7.6B**) correlated with innate pathway markers (IL-1β, IL-8, MIP-1α, and MIP-1β), reflecting the pro-inflammatory effect of the disturbed lipid metabolism. ROS-catalyzed lipid peroxidation products correlated almost exclusively with IP-10, part of the IFN-α pathway (**Fig. 7.6A**). The levels of IL-4, IL-5, IL-13, IL-17A, IL-18 and IFN-α and IFN-γ were below the detection limit of the sensitive multiplex bead assay in cord blood. C-reactive protein (CRP) was also assessed as this is a classical clinical marker for inflammation, however the concentration of CRP was more than 3 log lower than the clinically.

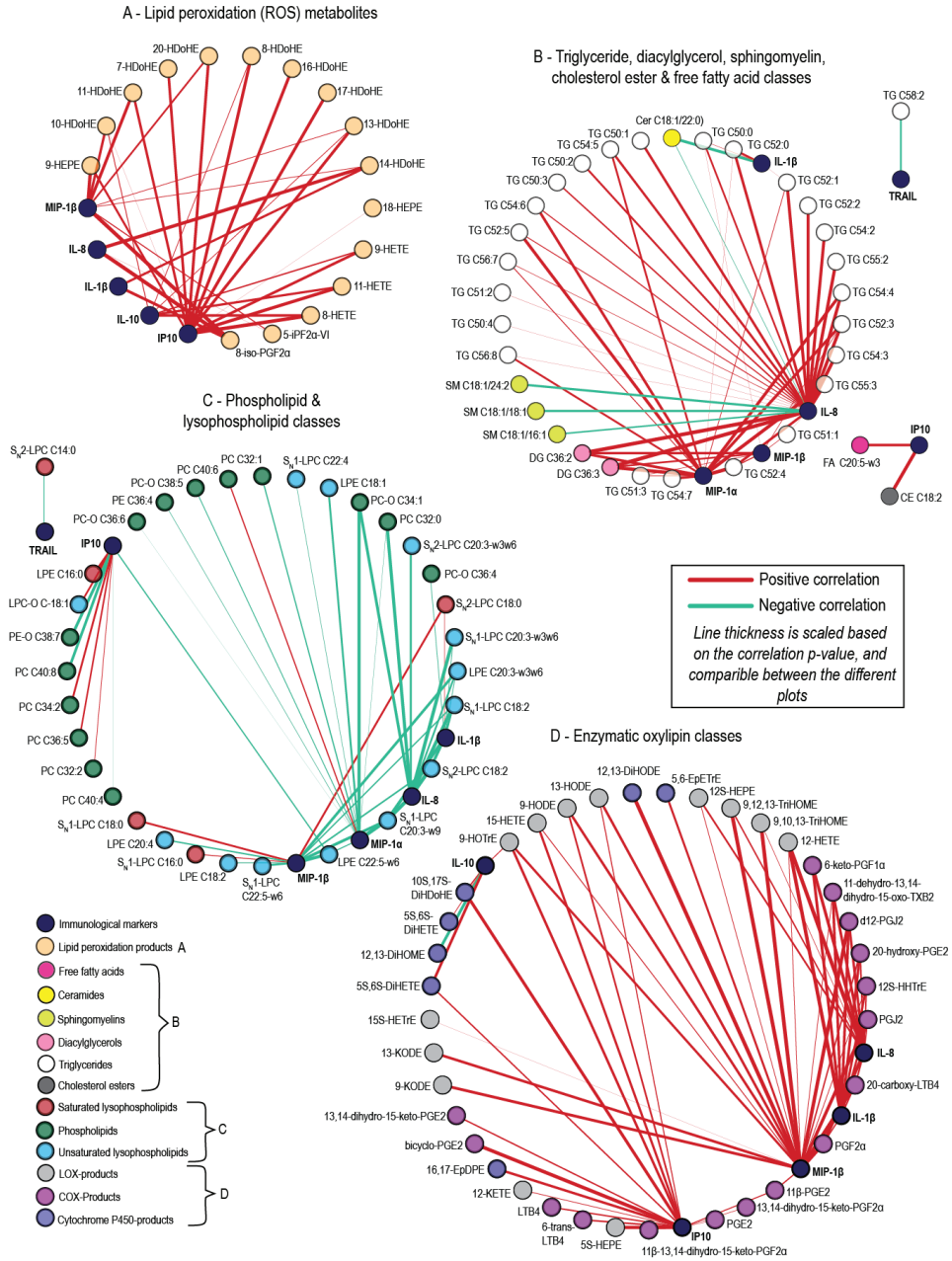

Figure 7.6: Pearson's correlation networks illustrating the correlation between metabolite classes and classic immunological markers. The correlation network shows the correlations ($p < 0.05$) between the measured cytokines and chemokines and the normalized metabolites for: (A) ROS lipid peroxidation metabolites; (B) triglycerides, sphingomyelins, diacylglycerols, cholesteryl esters, and free fatty acids; (C) phospholipids and lysophospholipids; and (D) enzymatic oxylipins.

relevant cut-off and not significantly different between the 2 groups (median cART-exposed HEU infants = 0.00012 mg/mL and median HUU infants = 0.00009 mg/mL $p = 0.547$). Low concentration of these cytokines

and chemokines is a well-known phenomenon in newborn infants. Together these data suggest the role of two separate pathways: first, changes in lipid metabolism and subsequent ER stress are correlated with increased activation of the MIP-1α and β, IL-1β and IL-8 pathways; in the second pathway, mitochondrial dysfunction increases the production of ROS and peroxidized lipids, which are associated with the IFN-α pathway. Both pathways were correlated with enzymatic oxylipins (**Fig. 7.6D**), saturated lysophospholipids (**Fig. 7.6C**), unsaturated lysophospholipids (**Fig. 7.6C**), and sphingomyelins (**Fig. 7.6B**), all of which are reflective of the pro-inflammatory milieu resulting from cell stress.

Discussion

Here, we investigated the impact of *in utero* cART-HIV exposure on lipid metabolism and mitochondrial functioning in uninfected infants born to HIV-infected women, using novel metabolomics tools. The metabolite profile observed in HEU infants exposed to long-term cART *in utero* is characterized by cell stress and dysregulation of metabolites with immune modulatory capacities, ultimately leading to a pro-inflammatory milieu in these infants. Specifically, we detected elevated levels of ROS-catalyzed lipid peroxidation products, increased levels of triglycerides and decreased levels of phospholipids. Mitochondrial dysfunction has been recognized as an adverse effect of NRTI's, and in particular of stavudine and zidovudine, which are actively transported across the placenta and can be detected in fetal blood and amniotic fluid [63]. NRTIs inhibit mtDNA replication [64], while indirectly affecting the electron transport chain's complexes assembling. The augmented peroxidized lipids provide a robust assessment of the consequences *in vivo* of the mitochondrial dysfunction due to NRTIs in HEU infants.

In addition, the lipid metabolome of cART-exposed HEU infants was also significantly differed from HUU infants (**Fig. 7.7**), including high triglycerides at levels similar to patients who are treated with PIs. As PIs are not actively transported across the placenta and detected at lower concentrations in cord blood [65,66], it had been assumed that PIs have a minimal effect on the developing fetus. The reduced levels of CYP4A and CYP2B6 eicosanoids in cART-exposed HEU infants however support a direct effect of PIs on fetal cells. Protease inhibitors—in particularly ritonavir, a booster that is often added to other PIs such as lopinavir and used for maternal treatment in this study— have been previously shown to inhibit CYP enzyme activity [67]. Next to PIs, stavudine or abacavir in combination with lamivudine can also induce hypertriglyceridemia, although the cART-exposed HEU infants were exposed to lamivudine in combination with zidovudine, the NRTI exposure may have further exacerbated triglyceride levels [68]. Of note, triglyceride levels in the black population are lower compared to the white population, as more black infants were HEU compared to the HUU infants, the increased triglycerides in these HEU infants could therefore be an underestimation of the impact of *in utero* cART exposure [69,70]. The observed altered lipid metabolome of cART-exposed HEU infants in this study provides the first report that *in utero* exposure to PIs can alter the lipid profile and CYP enzyme activity in the fetus.

Furthermore, our results show that alterations in metabolite profile due to antiretroviral drugs can induce cell stress modulating immune responses. Lipid peroxidation products positively correlated with IP-10.

The role of ROS in activation of the inflammasome is well known, however ROS can also induce metabolic stress by inhibiting the sarco/endoplasmic reticulum calcium transport ATPase (SERCA) pump [71,72], thereby disabling the ER's central role in Ca^{2+} homeostasis and activating ER stress signaling pathways (e.g., the PERK pathway) and the production of IP-10 (**Fig. 7.7**). Additionally, hypertriglyceridemia and the resulting disrupted ER membrane homeostasis - illustrated by reduced phosphatidylcholine levels in cART-exposed HEU infants - activate the ER stress-induced UPR. UPR induces the translocation of NF-κB to the nucleus and transcription of proinflammatory gene products (**Fig. 7.7**), including IL-1β, IL-8, MIP-1α, and MIP1β, which were associated with triglycerides and saturated lysophosphatidylethanolamines and lysophosphatidylcholine levels in cART-exposed HEU infants. Lastly, significantly lower levels of the potent anti-inflammatory arachidonic acid–derived CYP metabolites were detected in cART-exposed HEU infants, reducing compensatory homeostatic mechanisms in the infants. Taken together, the metabolic perturbations in cART-exposed HEU infants were characterized by an altered lipid metabolism and mitochondrial dysfunctioning, resulting in a pro-inflammatory milieu in cART-exposed HEU infants. Further studies are required to understand how these changes in metabolites and downstream immune responses provide the underlying conditions for the described increased susceptibility of cART-exposed HEU infants to intracellular pathogens [73–75]. However, immune inflammation does not equal immune competence as patients with inflammatory disease can have an increased susceptibility to infections. Skewing of immune responses away from T helper 1 (Th1), IFN-γ responses may contribute to this susceptibility in cART-exposed HEU infants [27].

Our results provide a novel framework for further studies identifying the precise mechanisms resulting in continuous low-level immune activation even in successfully cART-treated patients with an undetectable viral load [76]. The ongoing immune activation in these patients has been attributed to residual viral replication, activating immune cells, such as dendritic cells and monocytes as well as T and B cells [77–79]. The IFN-α pathway has been identified to play an important role in this ongoing immune activation and associated non-AIDS-related comorbidities. Although a separate effect of the maternal HIV-infection cannot be excluded, the results from uninfected infants here suggest that NRTIs, by inducing mitochondrial dysfunction, can activate the IFN-α pathway and contribute to low-level immune activation. Furthermore, PI-induced lipid perturbations eliciting ER stress may further aggravate immune activation via MIP-1α and β, IL-1β and IL-8 in virally suppressed HIV-1-infected individuals [76,77]. Investigating the role of drug-induced ER stress and inflammation may provide new insights to prevent ongoing immune activation in HIV-infected patients on cART. It is currently unclear whether the altered metabolism in cART-exposed HEU fetuses has long-term consequences either due to disturbed fetal development during exposure or due to long-lasting perturbations of metabolic pathways via for example epigenetic modifications [80]. After cessation of PI treatment in adults' triglyceride levels return to normal values, which suggests that this may also occur in the cART-exposed HEU infants. However, consequences of the altered lipid metabolism may reach beyond its effect on immune responses. Lipids are a critical component of the brain, and essential for early brain development [81]. Disturbance of lipids may affect brain development. Studies investigating long-term effects of *in utero* exposure to NRTI in patas monkeys furthermore showed abnormal mitochondrial morphology and altered mtDNA levels persisting for up to 3 years of age [82]. A recent study by Jao et al, showed that the acyl-carnitine profile and branched amino acids

were associated with an altered insulin metabolism in HEU infants at 6 weeks of age [83]. These mitochondrial abnormalities, underscore the need for further studies to assess whether changes in fetal metabolism resulting from exposure to drugs have long-term clinical consequences.

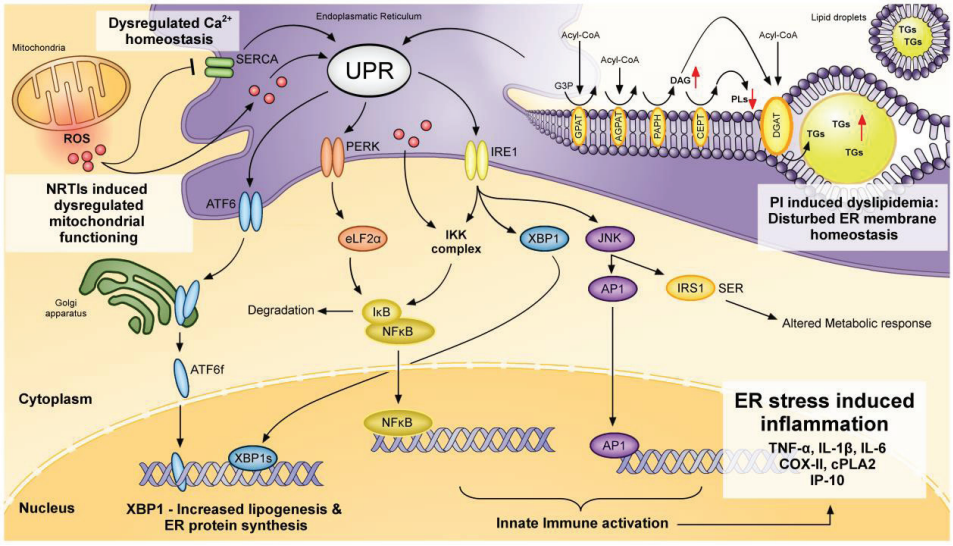

Figure 7.7: *In utero* metabolic changes due to cART exposure and the role of the ER in stress and innate signaling. Nucleotide reverse transcriptase inhibitor (NRTI)–induced mitochondrial dysfunction leads to increased levels of ROS, which are sensed by the ER. PI-induced lipid dysregulation leads to increased triglycerides (TGs) and decreased phospholipids (PLs), thereby disrupting ER membrane homeostasis. ER stress activates unfolded protein response (UPR) signaling via ATF6, PERK, and IRE1. Activated transcription factors translocate to the nucleus, where they activate both the proinflammatory innate immune response and pathways for lipogenesis.

Next to cART exposure, the infants were also exposed to the consequences of the maternal HIV-infection, which may have affected the infants' metabolome. The potential consequences of the two most important remaining changes in optimally treated HIV-infected patients - microbial translocation due to the reduced intestinal barrier and increased levels of type 1 interferons due to residual viral replication - will be discussed here, as they have been implicated in changes in triglyceride levels. LPS concentration in plasma has been reported to be associated with triglyceride levels in untreated HIV-infected patients and treated patients with lipodystrophy. Interestingly an association between LPS and triglycerides was not observed in cART treated HIV-infected individuals without lipodystrophy [84,85]. Since these infants were not infected nor did they have lipodystrophy, it seems less likely that LPS crossing the placenta induced the changes in the lipid metabolism in the fetus. Furthermore, type 1 interferons (IFN) can also interfere with the lipid metabolism. Treatment with PEG IFN-α of HIV and HCV co-infected patients has been described to lead to increased levels of triglycerides in some studies [86], [87]. Therapeutic concentrations of IFN-α are higher compared to *in vivo*

measured concentrations in virally suppressed HIV-infected patients. In addition, maternal cytokines in circulation are notoriously insufficiently transported across the placenta, even during bacterial placental inflammation. In addition, PIs, in particular ritonavir-boosted lopinavir to which the infants are exposed here, are more potent inducers of triglycerides compared to above described effects of microbial translocation and type 1 interferons [84–86]. Thus, although these indirect routes affecting lipid metabolism cannot be excluded, cART exposure is likely the main driver of dyslipidemia observed in the cART-exposed HEU infants and fits the complex metabolic phenotype of HEU infants. This concurs with several large cohort studies of HIV-infected women and their offspring showing that cART, viral load and maternal immune markers such as CD4 have separate effects in multivariable models on immune parameters in infants such as infant total lymphocyte count, CD4 count, CD8 count and IgG [88–90]. As the immune system of treated HIV-infected women more closely resembles the immune system of healthy women than untreated HIV-infected women and studies of cART-exposed infants born to healthy women are not feasible due to ethical reasons, we deemed it appropriate to compare cART-exposed HEU with HUU infants to determine the impact of cART on the fetal metabolism.

Our study investigating systemic immunometabolism in cART-exposed HEU infants is at the interface of immune and metabolic responses in health and disease and provides new insights in the modulatory capacity of metabolites of immune responses and their contribution to pathology. Moreover, these studies provide a unique opportunity to identify novel pathways and clinically relevant biomarkers, which can be targeted in order to treat specific diseases. Newly developed targeted metabolomics provide the tools to identify metabolites both quantitatively and qualitatively, with higher sensitivity than can be achieved using non-targeted methods such as nuclear-magnetic-resonance-based techniques (NMR). However, because not all metabolites are measured in the plasma, some metabolic information can potentially be missed. Since these targeted metabolomics approaches require only 5 - 150 μL plasma per platform, they are ideal for studies limited in sample volume such as infant studies, while still being able to measure a broad range of metabolites. Furthermore, the approach taken here using chemical compounds to quantify ROS production via lipid peroxidation, provides the opportunity to measure the actual consequences of produced ROS *in vivo*. Comparatively, measuring mitochondrial functioning at the extreme borders through *in vitro* stimulants and inhibitors using Seahorse technology doesn't reflect the physiological *in vivo* conditions in HEU infants. Taken together the metabolomics platforms used in this study provided the opportunity to assess metabolites reflecting the *in vivo* metabolic state in cART-exposed HEU infants and to identify pathways impacted by *in utero* cART exposure. Further *in vitro* mechanistic studies will be needed to fully understand the dysregulation of pathways that lead to the altered metabolism in cART-exposed HEU infants, and long-term follow-up studies are required to confirm our findings and determine whether these perturbations persist beyond infancy. The required sample size used in our study was informed by previously published work in patas monkeys as well as in cART-exposed HEU infant studies [91–93]. Testing of a large number of intermediate metabolites within a pathway increased the robustness and power of our analyses.

In conclusion, our results demonstrate extensive dysregulation of several metabolic pathways in infants with *in utero* exposure to cART and HIV, providing the underlying conditions for a pro-inflammatory milieu observed in these infants. These studies indicate that cART-exposure has a significant impact on cell

functioning at birth and may have long-lasting adverse effects. Although cART is critical in preventing MTCT of HIV, longitudinal studies assessing metabolic functioning in the infants and *in vitro* studies uncovering the underlying molecular pathways are required to design optimal prevention of MTCT of HIV regimens, with minimal adverse effects.

Acknowledgments

Firstly, we would like tto thank the women for participating in the study. We would like to thank K. Boer, M. Godfried and J. Nellen for care of the pregnant women and K. Boer for collection of the samples. J. Fu and V.V Koval for help with statistical data analyses. We would like to thank the technical staff at the NMC (Leiden University) for metabolics platform sample analyses and data processing. We would like to thank A. Drewniak, M. Janssen and J. van Hamme for help with the immunological assays. We also acknowledge A. Sagebiel for help rendering Figure 7. This study was supported by the NWO-ZonMW grant number 435002027, and the Virgo consortium, funded by the Dutch government project number FES0908.

References

1. Carpenter, C. C. *et al.* Antiretroviral therapy for HIV infection in 1996. Recommendations of an international panel. International AIDS Society-USA. *JAMA* **276,** 146–54 (1996).
2. Townsend, C. L. *et al.* Low rates of mother-to-child transmission of HIV following effective pregnancy interventions in the United Kingdom and Ireland, 2000-2006. *AIDS* **22,** 973–81 (2008).
3. Kouanda, S. *et al.* Impact of maternal HAART on the prevention of mother-to-child transmission of HIV: results of an 18-month follow-up study in Ouagadougou, Burkina Faso. *AIDS Care* **22,** 843–850 (2010).
4. Afran, L. *et al.* HIV-exposed uninfected children: a growing population with a vulnerable immune system? *Clin. Exp. Immunol.* **176,** 11–22 (2014).
5. Barret, B. *et al.* Persistent mitochondrial dysfunction in HIV-1-exposed but uninfected infants: clinical screening in a large prospective cohort. *AIDS* **17,** 1769–85 (2003).
6. von Mollendorf, C. *et al.* Increased risk and mortality of invasive pneumococcal disease in HIV-exposed-uninfected infants <1 year of age in South Africa, 2009-2013. *Clin. Infect. Dis.* **60,** 1346–56 (2015).
7. Adler, C. *et al.* Severe Infections in HIV-Exposed Uninfected Infants Born in a European Country. *PLoS One* **10,** e0135375 (2015).
8. Ackerman, W. & Kwiek, J. J. Role of the placenta in adverse perinatal outcomes among HIV-1 seropositive women. *J. Nippon Med. Sch.* **80,** 90–4 (2013).
9. Suy, A. *et al.* Increased risk of pre-eclampsia and fetal death in HIV-infected pregnant women receiving highly active antiretroviral therapy. *AIDS* **20,** 59–66 (2006).
10. Boyajian, T., Shah, P. S. & Murphy, K. E. Risk of preeclampsia in HIV-positive pregnant women receiving HAART: a matched cohort study. *J. Obstet. Gynaecol. Canada* **34,** 136–41 (2012).
11. Machado, E. S. *et al.* NIH Public Access. *Sex Transm Infect.* **85,** 82–87 (2009).
12. Senise, J. F., Castelo, A. & Martínez, M. Current treatment strategies, complications and considerations for the use of HIV antiretroviral therapy during pregnancy. *AIDS Rev.* **13,** 198–213 (2011).
13. Parekh, N. *et al.* Risk factors for very preterm delivery and delivery of very-small-for- gestational-age infants among HIV-exposed and HIV-unexposed infants in Botswana. *Int. J. Gynecol. Obstet.* **115,** 20–25 (2011).
14. Ivanovic, J. *et al.* Transplacental transfer of antiretroviral drugs and newborn birth weight in HIV-

infected pregnant women. *Curr. HIV Res.* **7,** 620–625 (2009).
15. Kirmse, B. *et al.* Abnormal newborn screens and acylcarnitines in HIV-exposed and ARV-exposed infants. *Pediatr. Infect. Dis. J.* **32,** 146–50 (2013).
16. Hernàndez, S. *et al.* Perinatal outcomes, mitochondrial toxicity and apoptosis in HIV-treated pregnant women and in-utero-exposed newborn. *Aids* **26,** 419–428 (2012).
17. Divi, R. L. *et al.* Mitochondrial damage and DNA depletion in cord blood and umbilical cord from infants exposed in utero to Combivir. *AIDS* **18,** 1013–21 (2004).
18. Blanche, S. *et al.* Persistent mitochondrial dysfunction and perinatal exposure to antiretroviral nucleoside analogues. *Lancet (London, England)* **354,** 1084–9 (1999).
19. Mandl, J., Mészáros, T., Bánhegyi, G., Hunyady, L. & Csala, M. Endoplasmic reticulum: nutrient sensor in physiology and pathology. *Trends Endocrinol. Metab.* **20,** 194–201 (2009).
20. Efeyan, A., Comb, W. C. & Sabatini, D. M. Nutrient-sensing mechanisms and pathways. *Nature* **517,** 302–10 (2015).
21. Harijith, A., Ebenezer, D. L. & Natarajan, V. Reactive oxygen species at the crossroads of inflammasome and inflammation. *Front. Physiol.* **5,** 352 (2014).
22. Hotamisligil, G. S. Endoplasmic Reticulum Stress and the Inflammatory Basis of Metabolic Disease. *Cell* **140,** 900–917 (2010).
23. Walter, P. & Ron, D. The unfolded protein response: from stress pathway to homeostatic regulation. *Science* **334,** 1081–6 (2011).
24. Fu, S. *et al.* Aberrant lipid metabolism disrupts calcium homeostasis causing liver endoplasmic reticulum stress in obesity. *Nature* **473,** 528–531 (2011).
25. Borges-Almeida, E. *et al.* The impact of maternal HIV infection on cord blood lymphocyte subsets and cytokine profile in exposed non-infected newborns. *BMC Infect. Dis.* **11,** 38 (2011).
26. Hygino, J. *et al.* Altered immunological reactivity in HIV-1-exposed uninfected neonates. *Clin. Immunol.* **127,** 340–7 (2008).
27. Bunders, M. J. *et al.* Fetal exposure to HIV-1 alters chemokine receptor expression by CD4+T cells and increases susceptibility to HIV-1. *Sci. Rep.* **4,** 6690 (2014).
28. Feiterna-Sperling, C. *et al.* Hematologic effects of maternal antiretroviral therapy and transmission prophylaxis in HIV-1-exposed uninfected newborn infants. *J. Acquir. Immune Defic. Syndr.* **45,** 43–51 (2007).
29. Tsalikis, J., Croitoru, D. O., Philpott, D. J. & Girardin, S. E. Nutrient sensing and metabolic stress pathways in innate immunity. *Cell. Microbiol.* **15,** 1632–1641 (2013).
30. Ramsay, G. & Cantrell, D. Environmental and Metabolic Sensors That Control T Cell Biology. *Front. Immunol.* **6,** 1–8 (2015).
31. Wang, R. & Green, D. R. Metabolic reprogramming and metabolic dependency in T cells. *Immunol. Rev.* **249,** 14–26 (2012).
32. Klysz, D. *et al.* Glutamine-dependent a -ketoglutarate production regulates the balance between T helper 1 cell and regulatory T cell generation. *Sci. Signal.* **8,** 1–13 (2015).
33. Buck, M. D., O'Sullivan, D. & Pearce, E. L. T cell metabolism drives immunity. *J. Exp. Med.* **212,** 1345–1360 (2015).
34. Lochner, M., Berod, L. & Sparwasser, T. Fatty acid metabolism in the regulation of T cell function. *Trends Immunol.* **36,** 81–91 (2015).
35. Strassburg, K. *et al.* Quantitative profiling of oxylipins through comprehensive LC-MS/MS analysis: application in cardiac surgery. *Anal. Bioanal. Chem.* **404,** 1413–26 (2012).
36. Hu, C. *et al.* RPLC-ion-trap-FTMS method for lipid profiling of plasma: method validation and application to p53 mutant mouse model. *J. Proteome Res.* **7,** 4982–91 (2008).
37. Xia, J., Sinelnikov, I. V., Han, B. & Wishart, D. S. MetaboAnalyst 3.0—making metabolomics more meaningful. *Nucleic Acids Res.* **43,** W251–W257 (2015).
38. Shannon, P. *et al.* Cytoscape: a software environment for integrated models of biomolecular interaction networks. *Genome Res.* **13,** 2498–504 (2003).
39. Pusukuru, R. *et al.* Evaluation of Lipid Profile in Second and Third Trimester of Pregnancy. *J. Clin. Diagn. Res.* **10,** QC12-6 (2016).

40. Morrow, J. D. *et al.* A series of prostaglandin F2-like compounds are produced in vivo in humans by a non-cyclooxygenase, free radical-catalyzed mechanism. *Proc. Natl. Acad. Sci. U. S. A.* **87,** 9383–9387 (1990).
41. VanRollins, M. & Murphy, R. C. Autooxidation of docosahexaenoic acid: analysis of ten isomers of hydroxydocosahexaenoate. *J. Lipid Res.* **25,** 507–517 (1984).
42. Shishehbor, M. H. *et al.* Systemic elevations of free radical oxidation products of arachidonic acid are associated with angiographic evidence of coronary artery disease. *Free Radic. Biol. Med.* **41,** 1678–1683 (2006).
43. Kirkinezos, I. G. & Moraes, C. T. Reactive oxygen species and mitochondrial diseases. *Semin. Cell Dev. Biol.* **12,** 449–457 (2001).
44. Tsiodras, S., Mantzoros, C., Hammer, S. & Samore, M. Effects of protease inhibitors on hyperglycemia, hyperlipidemia, and lipodystrophy: a 5-year cohort study. *Arch. Intern. Med.* **160,** 2050–2056 (2000).
45. Feeney, E. R. & Mallon, P. W. G. HIV and HAART-Associated Dyslipidemia. *Open Cardiovasc. Med. J.* **5,** 49–63 (2011).
46. Parker, R. a *et al.* Endoplasmic reticulum stress links dyslipidemia to inhibition of proteasome activity and glucose transport by HIV protease inhibitors. *Mol. Pharmacol.* **67,** 1909–1919 (2005).
47. Zha, B. S. *et al.* HIV Protease Inhibitors Disrupt Lipid Metabolism by Activating Endoplasmic Reticulum Stress and Inhibiting Autophagy Activity in Adipocytes. *PLoS One* **8,** 1–16 (2013).
48. Vu, C. N. *et al.* Altered relationship of plasma triglycerides to HDL cholesterol in patients with HIV/HAART-associated dyslipidemia: Further evidence for a unique form of Metabolic Syndrome in HIV patients. *Metabolism.* **62,** 1014–1020 (2013).
49. Magnusson-Olsson, A. L., Lager, S., Jacobsson, B., Jansson, T. & Powell, T. L. Effect of maternal triglycerides and free fatty acids on placental LPL in cultured primary trophoblast cells and in a case of maternal LPL deficiency. *Am. J. Physiol. Endocrinol. Metab.* **293,** E24–E30 (2007).
50. Krahmer, N. *et al.* Phosphatidylcholine Synthesis for Lipid Droplet Expansion Is Mediated by Localized Activation of CTP:Phosphocholine Cytidylyltransferase. *Cell Metab.* **14,** 504–515 (2011).
51. Treede, I. *et al.* Anti-inflammatory effects of phosphatidylcholine. *J. Biol. Chem.* **282,** 27155–27164 (2007).
52. Hartmann, P. *et al.* Anti-inflammatory effects of phosphatidylcholine in neutrophil leukocyte-dependent acute arthritis in rats. *Eur. J. Pharmacol.* **622,** 58–64 (2009).
53. Lum, H. *et al.* Inflammatory stress increases receptor for lysophosphatidylcholine in human microvascular endothelial cells. *Am. J. Physiol. Heart Circ. Physiol.* **285,** H1786–H1789 (2003).
54. Aiyar, N. *et al.* Lysophosphatidylcholine induces inflammatory activation of human coronary artery smooth muscle cells. *Mol. Cell. Biochem.* **295,** 113–120 (2007).
55. Hung, N. D., Sok, D. E. & Kim, M. R. Prevention of 1-palmitoyl lysophosphatidylcholine-induced inflammation by polyunsaturated acyl lysophosphatidylcholine. *Inflamm. Res.* **61,** 473–483 (2012).
56. Liu-Wu, Y., Hurt-Camejo, E. & Wiklund, O. Lysophosphatidylcholine induces the production of IL-1beta by human monocytes. *Atherosclerosis* **137,** 351–357 (1998).
57. Liu, Y. *et al.* The antiinflammatory effect of laminar flow: the role of PPARgamma, epoxyeicosatrienoic acids, and soluble epoxide hydrolase. *Proc. Natl. Acad. Sci. U. S. A.* **102,** 16747–52 (2005).
58. Node, K. *et al.* Anti-inflammatory properties of cytochrome P450 epoxygenase-derived eicosanoids. *Science* **285,** 1276–1279 (1999).
59. Larsen, B. T., Campbell, W. B. & Gutterman, D. D. Beyond vasodilatation: non-vasomotor roles of epoxyeicosatrienoic acids in the cardiovascular system. *Trends Pharmacol. Sci.* **28,** 32–38 (2007).
60. Ng, V. Y. *et al.* Cytochrome P450 Eicosanoids are Activators of Peroxisome Proliferator-Activated Receptor Alpha (PPARα). *Eicosanoids* **35,** 1126–1134 (2007).
61. Gimbrone, M. a, Brock, a F. & Schafer, a I. Leukotriene B4 stimulates polymorphonuclear leukocyte adhesion to cultured vascular endothelial cells. *J. Clin. Invest.* **74,** 1552–1555 (1984).
62. Martin, T. R., Raugi, G., Merritt, T. L. & Henderson, W. R. Relative contribution of leukotriene B4 to the neutrophil chemotactic activity produced by the resident human alveolar macrophage. *J. Clin.*

Invest. **80,** 1114–1124 (1987).
63. Treluyer, J., Jullien, V., Rey, E., Fouche, M. & Firtion, G. Maternal-Fetal Transfer and Amniotic Fluid Accumulation of Nucleoside Analogue Reverse Transcriptase Inhibitors in Human Immunodeficiency Virus-Infected Pregnant Women. *Society* **48,** 4332–4336 (2004).
64. Johnson, A. A. *et al.* Toxicity of antiviral nucleoside analogs and the human mitochondrial DNA polymerase. *J. Biol. Chem.* **276,** 40847–57 (2001).
65. Yeh, R. F. *et al.* Genital tract, cord blood, and amniotic fluid exposures of seven antiretroviral drugs during and after pregnancy in human immunodeficiency virus type 1-infected women. *Antimicrob. Agents Chemother.* **53,** 2367–2374 (2009).
66. Marzolini, C. *et al.* Transplacental passage of protease inhibitors at delivery. *AIDS* **16,** 889–893 (2002).
67. von Moltke, L. L. *et al.* Protease inhibitors as inhibitors of human cytochromes P450: high risk associated with ritonavir. *J. Clin. Pharmacol.* **38,** 106–111 (1998).
68. Kamara, D. A. *et al.* Longitudinal analysis of the associations between antiretroviral therapy, viraemia and immunosuppression with lipid levels: the D:A:D study. *Antivir. Ther.* 3851 (2016). doi:10.3851/IMP3051
69. Ellman, N., Keswell, D., Collins, M., Tootla, M. & Goedecke, J. H. Ethnic differences in the association between lipid metabolism genes and lipid levels in black and white South African women. *Atherosclerosis* **240,** 311–317 (2015).
70. Garcia, A. E. *et al.* Lipoprotein profiles in class III obese Caucasian and African American women with nonalcoholic fatty liver disease. *PLoS One* **10,** 1–17 (2015).
71. Cook, N. L. *et al.* Myeloperoxidase-derived oxidants inhibit sarco/endoplasmic reticulum Ca2+-ATPase activity and perturb Ca2+ homeostasis in human coronary artery endothelial cells. *Free Radic. Biol. Med.* **52,** 951–61 (2012).
72. Zima, A. V. & Blatter, L. A. Redox regulation of cardiac calcium channels and transporters. *Cardiovasc. Res.* **71,** 310–21 (2006).
73. Marinda, E. *et al.* Child mortality according to maternal and infant HIV status in Zimbabwe. *Pediatr. Infect. Dis. J.* **26,** 519–26 (2007).
74. Koyanagi, A. *et al.* Morbidity among human immunodeficiency virus-exposed but uninfected, human immunodeficiency virus-infected, and human immunodeficiency virus-unexposed infants in Zimbabwe before availability of highly active antiretroviral therapy. *Pediatr. Infect. Dis. J.* **30,** 45–51 (2011).
75. Landes, M. *et al.* Mortality and health outcomes of HIV-exposed and unexposed children in a PMTCT cohort in Malawi. *PLoS One* **7,** e47337 (2012).
76. Netanya, U. S. *et al.* CROI 2015 : Inflammation Persists Despite Early Initiation of ART in Acute HIV Infection. *Croi 2015* 14–15 (2015).
77. Deeks, S. G. HIV Infection, Inflammation, Immunosenescence, and Aging. *Annu. Rev. Med.* **62,** 141–155 (2011).
78. Grossman, Z., Meier-Schellersheim, M., Paul, W. E. & Picker, L. J. Pathogenesis of HIV infection: what the virus spares is as important as what it destroys. *Nat. Med.* **12,** 289–295 (2006).
79. Anzinger, J. J., Butterfield, T. R., Angelovich, T. A., Crowe, S. M. & Palmer, C. S. Monocytes as regulators of inflammation and HIV-related comorbidities during cART. *Journal of Immunology Research* **2014,** (2014).
80. Desai, M. & Hales, C. N. Role of fetal and infant growth in programming metabolism in later life. *Biol. Rev. Camb. Philos. Soc.* **72,** 329–48 (1997).
81. Innis, S. M. Essential fatty acid transfer and fetal development. *Placenta* **26,** S70–S75 (2005).
82. Olivero, O. A. *et al.* Perinatal Exposure of Patas Monkeys to Antiretroviral Nucleoside Reverse-Transcriptase Inhibitors Induces Genotoxicity Persistent for up to 3 Years of Age. *J. Infect. Dis.* **208,** 244–248 (2013).
83. Jao, J. *et al.* Lower preprandial insulin and altered fuel use in HIV/antiretroviral-exposed infants in Cameroon. *J. Clin. Endocrinol. Metab.* **100,** 3260–3269 (2015).
84. Viladés, C. *et al.* Involvement of the LPS-LPB-CD14-MD2-TLR4 inflammation pathway in HIV-1/HAART-associated lipodystrophy syndrome (HALS). *J. Antimicrob. Chemother.* **69,** 1653–9 (2014).

85. Timmons, T. *et al.* Microbial translocation and metabolic and body composition measures in treated and untreated HIV infection. *AIDS Res. Hum. Retroviruses* **30,** 272–7 (2014).
86. Butt, A. A., Umbleja, T., Andersen, J. W., Sherman, K. E. & Chung, R. T. Impact of Peginterferon Alpha and Ribavirin Treatment on Lipid Profiles and Insulin Resistance in Hepatitis C Virus/HIV-Coinfected Persons: The AIDS Clinical Trials Group A5178 Study. *Clin. Infect. Dis.* **55,** 631–638 (2012).
87. Jung, H. J. *et al.* The impact of pegylated interferon and ribavirin combination treatment on lipid metabolism and insulin resistance in chronic hepatitis C patients. *Clin. Mol. Hepatol.* **20,** 38–46 (2014).
88. Bunders, M., Thorne, C., Newell, M. L. & European Collaborative Study. Maternal and infant factors and lymphocyte, CD4 and CD8 cell counts in uninfected children of HIV-1-infected mothers. *AIDS* **19,** 1071–9 (2005).
89. Bunders, M., Pembrey, L., Kuijpers, T. & Newell, M.-L. Evidence of impact of maternal HIV infection on immunoglobulin levels in HIV-exposed uninfected children. *AIDS Res. Hum. Retroviruses* **26,** 967–75 (2010).
90. Le Chenadec, J., Mayaux, M.-J., Guihenneuc-Jouyaux, C., Blanche, S. & Enquête Périnatale Française Study Group. Perinatal antiretroviral treatment and hematopoiesis in HIV-uninfected infants. *AIDS* **17,** 2053–61 (2003).
91. Gerschenson, M. *et al.* Mitochondrial Toxicity in Fetal Erythrocebus patas Monkeys Exposed Transplacentally to Zidovudine Plus Lamivudine. *AIDS Res. Hum. Retroviruses* **20,** 91–100 (2004).
92. Divi, R. L. *et al.* Cardiac mitochondrial compromise in 1-yr-old Erythrocebus patas monkeys perinatally-exposed to nucleoside reverse transcriptase inhibitors. *Cardiovasc. Toxicol.* **5,** 333–46 (2005).
93. Andre-Schmutz, I. *et al.* Genotoxic Signature in Cord Blood Cells of Newborns Exposed In Utero to a Zidovudine-Based Antiretroviral Combination. *J. Infect. Dis.* **208,** 235–243 (2013).

Chapter 7 Supplementary information

Table S7.1: Clinical information of the HIV-infected pregnant mothers who received cART

Mothers		Viral Load (copies/mL)			CD4 count (10E6 cells/L)				Days on ART treatment till infant DOB					
Age (y)	Ethnicity	1st trimester	2nd trimester	3rd trimester	NADIR#	1st trimester	2nd trimester	3rd trimester	Zidovudine + Lamivudine	Lopinavir + ritonavir	Nelfinavir	Nevirapine	Tenofovir	Saquinavir
38	White	0	0	0	180	420	380	380	0	377	0	377	0	377
33	Black	0	0	0	200	540	460	500	331	0	331	0	0	0
39	Black	0	0	0	720	790	720	850	329	0	0	0	0	0
28	White	4244	65	0	720	720	910	1050	129	24	105	0	0	0
29	Black	829	1180	0	450	450	460	590	489	29	460	0	0	0
26	Black	0	0	0	250	830	770	830	223	0	0	458	109*	0
32	White	228	153	0	690	690	920	1170	111	87	25	0	0	0
28	Black	39419	279	0	290	290	390	500	138	92	46	0	0	0
39	Black	8863	196	0	450	450	550	700	113	95	18	0	0	0
24	Black	4573	54	0	440	440	500	710	161	111	50	0	0	0
26	Black	0	0	0	210	460	540		490	0	0	490	0	0
21	Black	3963	46	0	290	290	380	470	120	120	0	0	0	0

* Tenofovir was discontinued in the 1st trimester of pregnancy

NADIR - Lowest CD4 count

Table S7.2: Metabolites identified as significantly different between *in utero* cART- and HIV-exposed (HEU) infants and HUU control infants. Selected metabolites for biological interpretation adhering to the predefined univariate scores criteria for the cART-exposed HEU infants and HUU infants.

			Univariate comparison		Descriptive statistics			
					HUU infants		cART-exposed HEU infants	
Targeted Metabolomics platform	**Metabolite class**	**Metabolite**	**MW t-test (p – value)**	**Fold Change (FC)**	**Mean (SD)**	**Median (Range)**	**Mean (SD)**	**Median Range)**
Oxylipins Platform	Non-enzymatic Oxylipins	10-HDoHE	0.041	4.13	3.25 (1.41)	1.89 (5.83)	4.31 (2.73)	4.32 (7.35)
		11-HDoHE	0.013	5.43	19.37 (12.04)	15.79 (45.07)	37.63 (21.14)	37.01 (64.95)
		11-HETE	0.028	3.71	4.31 (2.44)	3.63 (8.18)	8.34 (5.1045)	7.86 (17.3)
		16-HDoHE	0.019	5.04	2.33 (1.29)	2.22 (5.11)	4.51 (2.6757)	4.86 (7.33)
		17-HDoHE	0.017	5.53	6.00 (2.59)	6.06 (9.51)	11.76 (5.2)	13.65 (13.50)
		20-HDoHE	0.042	3.52	2.32 (0.9)	1.51 (3.11)	3.03 (1.73)	2.75 (5.22)
		4-HDoHE	0.014	5.55	10.36 (5.46)	9.05 (17.53)	16.28 (8.51)	15.76 (28.05)
		7-HDoHE	0.017	6.66	0.16 (0.10)	0.13 (0.31)	0.37 (0.29)	0.28 (0.92)
		8_HDoHE	0.024	5.06	0.15 (0.08)	0.13 (0.29)	0.37 (0.27)	0.30 (0.78)
		8-HETE	0.02	3.3	2.74 (1.61)	2.26 (5.17)	5.03 (2.66)	5.06 (8.09)
		9-HEPE	0.04	5.29	0.03 (0.0247)	0.02 (0.08)	0.10 (0.08)	0.06 (0.22)
		9-HETE	0.044	3.15	3.80 (2.69)	3.37 (11.54)	7.63 (4.3829)	7.81 (12.09)
		8-iso-PGF2α	0.049	2.40	3.59 (2.35)	3.23 (10.20)	7.78 (5.02)	7.51 (14.54)
Positive Lipid platform	Diacylglycerols	DG (36:2)	0.0008	1.47	0.27 (0.05)	0.27 (0.14)	0.39 (0.13)	0.36 (0.45)
		DG (36:3)	0.001	1.61	0.19 (0.06)	0.18 (0.2)	0.30 (0.11)	0.29 (0.39)
Positive Lipid Platform	Triglycerides	TG (48:0)	0.011	2.2	0.24 (0.13)	0.22 (0.43)	0.54 (0.35)	0.42 (0.92)
		TG (48:1)	0.013	2.05	0.71 (0.42)	0.57 (1.32)	1.45 (1.04)	1.45 (3.93)
		TG (48:2)	0.011	2.12	0.48 (0.3)	0.44 (0.95)	1.02 (0.79)	0.96 (3)
		TG (48:3)	0.003	2.47	0.1 (0.06)	0.09 (0.21)	0.25 (0.17)	0.22 (0.65)
		TG (50:0)	0.005	1.87	0.21 (0.08)	0.22 (0.29)	0.39 (0.19)	0.36 (0.55)
		TG (50:1)	0.018	1.73	2.73 (1.28)	2.44 (4.76)	4.71 (2.62)	4.12 (7.51)
		TG (50:2)	0.019	1.66	3.69 (1.66)	3.5 (5.91)	6.14 (3.15)	6.02 (9.93)
		TG (50:3)	0.006	1.85	1.36 (0.61)	1.3 (1.88)	2.52 (1.19)	2.23 (3.51)
		TG (50:4)	0.002	2.05	0.23 (0.1)	0.23 (0.35)	0.47 (0.21)	0.46 (0.64)
		TG (51:1)	0.008	1.95	0.1 (0.06)	0.1 (0.21)	0.2 (0.12)	0.2 (0.43)
		TG (51:2)	0.016	1.85	0.19 (0.1)	0.16 (0.31)	0.35 (0.23)	0.3 (0.87)
		TG (51:3)	0.009	1.89	0.11 (0.06)	0.09 (0.17)	0.21 (0.11)	0.18 (0.38)
		TG (52:0)	0.001	2.06	0.04 (0.03)	0.03 (0.1)	0.09 (0.04)	0.09 (0.12)
		TG (52:1)	0.001	1.8	0.91 (0.33)	0.89 (0.96)	1.63 (0.65)	1.67 (1.95)
		TG (52:2)	0.009	1.59	5.93 (2.2)	6.26 (7.92)	9.42 (4.23)	8.85 (11.93)
		TG (52:3)	0.004	1.77	5.34 (2.25)	5.02 (7.34)	9.43 (4.21)	8 (11.71)
		TG (52:4)	0.003	1.99	1.77 (1.01)	1.34 (3.35)	3.52 (1.8)	3.07 (5.37)
		TG (52:5)	0.002	2.08	0.41 (0.16)	0.41 (0.56)	0.85 (0.4)	0.86 (1.26)
		TG (54:1)	0.008	1.67	0.08 (0.04)	0.07 (0.13)	0.13 (0.06)	0.13 (0.22)
		TG (54:2)	0.002	1.53	0.66 (0.26)	0.59 (0.89)	1.01 (0.32)	1.03 (0.96)
		TG (54:3)	0.007	1.44	1.47 (0.65)	1.44 (2.61)	2.11 (0.71)	2.02 (2.12)

		TG (54:4)	0.008	1.51	1.26 (0.72)	1.21 (2.96)	1.9 (0.7)	1.97 (2.07)
		TG (54:5)	0.005	1.74	1.15 (0.55)	1.03 (2.04)	2.01 (0.92)	1.76 (2.46)
		TG (54:6)	0.005	1.93	0.69 (0.31)	0.62 (1.08)	1.33 (0.7)	1.06 (1.97)
		TG (54:7)	0.012	2.01	0.17 (0.1)	0.17 (0.36)	0.35 (0.2)	0.27 (0.64)
		TG (55:2)	0.016	1.39	0.15 (0.05)	0.15 (0.15)	0.21 (0.07)	0.21 (0.19)
		TG (55:3)	0.004	1.5	0.15 (0.05)	0.15 (0.18)	0.22 (0.07)	0.2 (0.2)
		TG (56:7)	0.014	1.99	0.59 (0.38)	0.58 (1.2)	1.18 (0.67)	0.94 (1.98)
		TG (56:8)	0.011	1.86	0.34 (0.2)	0.33 (0.65)	0.63 (0.34)	0.48 (0.94)
		TG (58:6)	0.028	1.55	0.08 (0.04)	0.06 (0.13)	0.12 (0.06)	0.11 (0.18)
Positive Lipid Platform	Phospholipids	PC (32:0)	0.002	0.71	1.11 (0.29)	1.19 (0.79)	0.79 (0.22)	0.72 (0.67)
		PC (32:1)	0.029	0.69	0.98 (0.38)	0.89 (1.17)	0.67 (0.6)	0.58 (2.29)
		PC (36:3)	0.009	0.73	5.74 (1.53)	5.52 (5.65)	4.21 (1.39)	3.96 (4.79)
		PC (40:6)	0.004	1.55	1.28 (0.36)	1.42 (1.2)	1.98 (0.66)	1.97 (2.3)
		PC (O-34:1)	0.007	0.66	0.26 (0.08)	0.28 (0.24)	0.18 (0.06)	0.15 (0.18)
		PC (O-36:4)	0.012	0.77	0.55 (0.14)	0.51 (0.44)	0.43 (0.08)	0.41 (0.3)
		PE (38:4)	0.027	0.79	0.17 (0.04)	0.16 (0.13)	0.13 (0.04)	0.13 (0.15)
Negative lipid Platform	Lyso-phospholipids	SN1-LPC (18:0)	0.006	1.54	2.21 (0.61)	2.24 (2.14)	3.39 (1.38)	3.14 (4.49)
		SN1-LPC (20:3-w9)	0.003	0.51	0.01 (0.007)	0.01 (0.02)	0.006 (0.005)	0.004 (0.01)
		SN2-LPC (18:0)	0.003	1.54	0.23 (0.06)	0.23 (0.21)	0.36 (0.13)	0.33 (0.43)
		LPE (16:0)	0.015	1.32	0.08 (0.02)	0.07 (0.05)	0.11 (0.03)	0.11 (0.11)
		LPE (18:0)	0.009	1.38	0.09 (0.01)	0.09 (0.05)	0.11 (0.04)	0.11 (0.14)
Oxylipins Platform	COX, LOX, CYP Oxylipins	10S,17S-DiHDoHE	0.018	5.12	0.04 (0.04)	0.02 (0.14)	0.06 (0.053)	0.05 (0.18)
		11,12-DiHETrE	0.001	0.18	0.094 (0.025)	0.09 (0.11)	0.07 (0.018)	0.057 (0.06)
		19,20-EpDPE	0.008	6.6	95.1 (33.7)	102.3 (130.3)	121.78 (33.51)	135.1 (116.9)
		20-carboxy-LTB4	0.032	1.61	0.08 (0.05)	0.05 (0.16)	0.09 (0.08)	0.05 (0.22)
		5,6-DiHETrE	<0.0001	0.25	0.04 (0.013)	0.04 (0.05)	0.02 (0.013)	0.016 (0.034)
		5S-HEPE	0.04	5.68	3.94 (2.01)	4.13 (6.67)	9.97 (8.03)	7.06 (24.17)
		8,9-DiHETrE	<0.0001	0.18	0.054 (0.015)	0.051 (0.04)	0.02 (0.02)	0.013 (0.054)
		9-HOTrE	0.023	3.53	3.29 (1.94)	3.19 (8.79)	7.23 (4.66)	7.12 (12.61)

DG – Diacylglycerol; TG – Triglyceride; PC – Phosphatidylcholine; PC (O) – Plasmalogen phosphatidylcholine; PE – Phosphatidylethanolamine; LPC – Lysophosphatidylcholine; LPE – Lysophosphatidylethanolamine.

Table S7.3: Pearson's correlation analysis results of significant ROS oxylipin correlations with classic immunological markers.

Platform	Class	Metabolite	Pearson Correlation	p value (2-tailed)	N	Type of correlation (Pos/Neg)	Immunological marker	Immune pathway
Oxylipins	ROS	10-HDoHE	.471*	.049	18	Pos	IP10	IFNa pathway
		18-HEPE	.473*	.048	18	Pos		
		9-HEPE	.540*	.021	18	Pos		
		11-HDoHE	.551*	.018	18	Pos		
		9-HETE	.562*	.015	18	Pos		
		7-HDoHE	.563*	.015	18	Pos		
		13-HDoHE	.580*	.012	18	Pos		
		20-HDoHE	.580*	.012	18	Pos		
		8_HDoHE	.581*	.011	18	Pos		
		16-HDoHE	.582*	.011	18	Pos		
		17-HDoHE	.592**	.010	18	Pos		
		11-HETE	.605**	.008	18	Pos		
		8-HETE	.651**	.003	18	Pos		
		13-HDoHE	.487*	.041	18	Pos	IL-10	Inflammasone/ Innate Pathway
		8_HDoHE	.488*	.040	18	Pos		
		10-HDoHE	.494*	.037	18	Pos		
		9-HETE	.511*	.030	18	Pos		
		11-HETE	.543*	.020	18	Pos		
		8-HETE	.561*	.015	18	Pos		
		14-HDoHE	.542*	.020	18	Pos	IL-1beta	
		8-iso-PGF2a	.576*	.012	18	Pos		
		5-iPF2a-VI	.472*	.048	18	Pos	IL-8	
		14-HDoHE	.621**	.006	18	Pos		
		8-iso-PGF2a	.683**	.002	18	Pos		
		5-iPF2a-VI	.498*	.035	18	Pos	MIP-1beta	
		20-HDoHE	.523*	.026	18	Pos		
		10-HDoHE	.554*	.017	18	Pos		
		11-HDoHE	.583*	.011	18	Pos		
		9-HEPE	.632**	.005	18	Pos		
		8-iso-PGF2a	.730**	.001	18	Pos		
		13-HDoHE	.843**	.000	18	Pos		
		14-HDoHE	.849**	.000	18	Pos		

Table S7.4: Pearson's correlation analysis results of significant lipid metabolite (triglycerides, sphingomyelins, ceramides, cholesteryl esters, and free fatty acids) correlations with classic immunological markers.

Platform	Class	Metabolite	Pearson Correlation	p value (2-tailed)	N	Type of correlation (Pos/Neg)	Immunological marker	Immune pathway
Negative mode Lipids	Free fatty acid	FA (20:5-w3)	.547*	.015	19	Pos	IP10	IFNa pathway
Positive mode Lipid	Cholestrol-ester	CE (18:2)	.614**	.005	19	Pos		
	Ceramide	Cer (d18:1/22:0)	-.562*	.012	19	Neg	IL-1beta	Inflammasone/ Innate Pathway
		Cer (d18:1/22:0)	-.471*	.042	19	Neg	IL-8	
	Diacylglycerol	DG (36:3)	.681**	.001	19	Pos		
		DG (36:2)	.690**	.001	19	Pos		
		DG (36:2)	.550*	.015	19	Pos	MIP-1alfa	
		DG (36:3)	.621**	.005	19	Pos		
		DG (36:3)	.507*	.027	19	Pos	MIP-1beta	
		DG (36:2)	.542*	.017	19	Pos		
	Sphingomyelin	SM (d18:1/16:1)	-.502*	.028	19	Neg	IL-8	
		SM (d18:1/18:1)	-.527*	.020	19	Neg		
		SM (d18:1/24:2)	-.528*	.020	19	Neg		
	Triglyceride	TG (52:1)	.458*	.048	19	Pos	IL-1beta	
		TG (50:0)	.467*	.044	19	Pos		
		TG (52:0)	.524*	.021	19	Pos		
		TG (56:8)	.457*	.049	19	Pos	IL-8	
		TG (50:4)	.459*	.048	19	Pos		
		TG (51:1)	.459*	.048	19	Pos		
		TG (51:2)	.463*	.046	19	Pos		
		TG (56:7)	.468*	.043	19	Pos		
		TG (52:5)	.482*	.037	19	Pos		
		TG (54:6)	.482*	.036	19	Pos		
		TG (50:3)	.497*	.030	19	Pos		
		TG (50:0)	.506*	.027	19	Pos		
		TG (50:2)	.512*	.025	19	Pos		
		TG (54:5)	.528*	.020	19	Pos		
		TG (50:1)	.539*	.017	19	Pos		
		TG (52:4)	.539*	.017	19	Pos		
		TG (52:0)	.546*	.016	19	Pos		
		TG (52:1)	.577**	.010	19	Pos		
		TG (52:2)	.577**	.010	19	Pos		

TG (54:2)	.577**	.010	19	Pos	
TG (55:2)	.579**	.009	19	Pos	
TG (54:4)	.581**	.009	19	Pos	
TG (52:3)	.591**	.008	19	Pos	
TG (54:3)	.598**	.007	19	Pos	
TG (55:3)	.606**	.006	19	Pos	
TG (52:0)	.462*	.046	19	Pos	
TG (52:1)	.474*	.040	19	Pos	
TG (51:3)	.475*	.040	19	Pos	
TG (56:7)	.479*	.038	19	Pos	
TG (56:8)	.512*	.025	19	Pos	
TG (54:5)	.513*	.025	19	Pos	
TG (54:7)	.542*	.017	19	Pos	MIP-1alfa
TG (54:6)	.543*	.016	19	Pos	
TG (52:3)	.562*	.012	19	Pos	
TG (54:4)	.573*	.010	19	Pos	
TG (52:5)	.575*	.010	19	Pos	
TG (55:3)	.598**	.007	19	Pos	
TG (52:4)	.631**	.004	19	Pos	
TG (50:0)	.457*	.049	19	Pos	
TG (51:3)	.468*	.043	19	Pos	
TG (52:3)	.468*	.043	19	Pos	MIP-1beta
TG (51:1)	.471*	.042	19	Pos	
TG (52:4)	.482*	.036	19	Pos	
TG (58:2)	-.505*	.027	19	Neg	TRAIL

Table S7.5: Pearson's correlation analysis results of significant phospholipid metabolite correlations with classic immunological markers

Platform	Class	Metabolite	Pearson Correlation	p value (2-tailed)	N	Type of correlation (Pos/Neg)	Immunological marker	Immune pathway
Positive mode Lipids	Phospholipids	PC(40:4)	-.462*	.046	19	Neg	IP10	IFNa pathway
		PC(O-36:6)	.464*	.046	19	Pos		
		PC(32:2)	.477*	.039	19	Pos		
		PC(36:5)	.502*	.028	19	Pos		
		PC(34:2)	.516*	.024	19	Pos		
		PC(40:8)	-.548*	.015	19	Neg		
		PE(O-38:7)	-.565*	.012	19	Neg		
		PC(O-36:4)	-.476*	.039	19	Neg	IL-1beta	Inflammasone/ Innate Pathway
		PC(O-34:1)	-.565*	.012	19	Neg	IL-8	
		PC(32:0)	-.581**	.009	19	Neg		
		PC(O-36:6)	-.460*	.048	19	Neg	MIP-1alfa	
		PC(32:0)	-.464*	.045	19	Neg		
		PE(36:4)	-.471*	.042	19	Neg		
		PC(O-38:5)	-.478*	.038	19	Neg		
		PC(40:6)	.488*	.034	19	Neg		
		PC(32:1)	-.491*	.033	19	Neg		
		PC(O-34:1)	-.580**	.009	19	Neg		

Table S7.6: Pearson's correlation analysis results of significant lysophospholipid metabolite correlations with classic immunological markers

Platform	Class	Metabolite	Pearson Correlation	p value (2-tailed)	N	Type of correlation (Pos/Neg)	Immunological marker	Immune pathway
Negative mode Lipids	Lyso-phopholipids	LPE (22:5-w6)	-.489*	.034	19	Neg	IP10	IFNa pathway
		LPC (O-18:1)	.510*	.026	19	Pos		
		LPE (16:0)	.616**	.005	19	Pos		
		SN2-LPC (18:0)	.471*	.042	19	Pos	IL-1beta	Inflammasone/ Innate Pathway
		SN1-LPC (20:3-w3w6)	-.472*	.041	19	Neg		
		LPE (20:3-w3w6)	-.473*	.041	19	Neg		
		SN1-LPC (18:2)	-.520*	.022	19	Neg		
		SN2-LPC (18:2)	-.556*	.013	19	Neg		
		SN1-LPC (20:3-w9)	-.579**	.009	19	Neg		
		LPE (20:3-w3w6)	-.508*	.027	19	Neg	IL-8	
		SN2-LPC (20:3)-w3w6	-.522*	.022	19	Neg		
		SN1-LPC (20:3-w3w6)	-.594**	.007	19	Neg		
		SN1-LPC (18:2)	-.619**	.005	19	Neg		
		SN1-LPC (20:3-w9)	-.659**	.002	19	Neg		
		SN2-LPC (18:2)	-.664**	.002	19	Neg		
		SN1-LPC (22:4)	-.469*	.043	19	Neg	MIP-1alfa	
		LPE (22:5-w6)	-.484*	.036	19	Neg		
		LPE (18:1)	-.514*	.024	19	Neg		
		SN1-LPC (20:3-w9)	-.716**	.001	19	Neg		
		LPE (18:2)	-.479*	.038	19	Neg	MIP-1beta	
		SN1-LPC (16:0)	.482*	.037	19	Neg		
		LPE (20:4)	-.492*	.032	19	Neg		
		SN1-LPC (18:2)	-.492*	.032	19	Neg		
		SN2-LPC (18:2)	-.501*	.029	19	Neg		
		SN2-LPC (18:0)	.512*	.025	19	Pos		
		SN1-LPC (18:0)	.515*	.024	19	Pos		
		SN1-LPC (22:5-w6)	-.519*	.023	19	Neg		
		LPE (20:3-w3w6)	-.546*	.016	19	Neg		
		SN1-LPC (20:3-w9)	-.556*	.013	19	Neg		
		LPE (22:5-w6)	-.592**	.008	19	Neg		
		SN2-LPC (14:0)	-.480*	.037	19	Neg	TRAIL	

Table S7.7: Pearson's correlation analysis results of significant COX, LOX, and CYP oxylipin metabolite correlations with classic immunological markers

Platform	Class	Metabolite	Pearson Correlation	p value (2-tailed)	N	Type of correlation (Pos/Neg)	Immunological marker	Immune pathway
Oxylipins	COX	11beta-13,14-dihydro-15-keto-PGF2a	.476*	.046	18	Pos	IP10	IFNa pathway
		PGE2	.478*	.045	18	Pos		
		13,14-dihydro-15-keto-PGF2a	.484*	.042	18	Pos		
		11beta-PGE2	.500*	.035	18	Pos		
		13,14-dihydro-15-keto-PGE2	.512*	.030	18	Pos		
		bicyclo-PGE2	.644**	.004	18	Pos		
		PGF2a	.502*	.034	18	Pos	IL-1beta	Inflammasone/ Innate Pathway
		20-carboxy-LTB4	.511*	.030	18	Pos		
		PGJ2	.538*	.021	18	Pos		
		12S-HHTrE	.545*	.019	18	Pos		
		20-hydroxy-PGE2	.557*	.016	18	Pos		
		d12-PGJ2	.558*	.016	18	Pos		
		TXB2	.568*	.014	18	Pos		
		6-keto-PGF1a	.572*	.013	18	Pos		
		bicyclo-PGE2	.530*	.024	18	Pos	IL-6	
		PGJ2	.501*	.034	18	Pos	IL-8	
		12S-HHTrE	.509*	.031	18	Pos		
		20-carboxy-LTB4	.514*	.029	18	Pos		
		20-hydroxy-PGE2	.518*	.028	18	Pos		
		d12-PGJ2	.550*	.018	18	Pos		
		TXB2	.558*	.016	18	Pos		
		6-keto-PGF1a	.589*	.010	18	Pos		
		PGF2a	.624**	.006	18	Pos		
		11beta-PGE2	.505*	.033	18	Pos	MIP-1beta	
		20-hydroxy-PGE2	.512*	.030	18	Pos		
		PGJ2	.597**	.009	18	Pos		
		d12-PGJ2	.663**	.003	18	Pos		
		PGF2a	.715**	.001	18	Pos		
		20-carboxy-LTB4	.719**	.001	18	Pos		
		TXB2	.800**	.000	18	Pos		
		12S-HHTrE	.811**	.000	18	Pos		

	16,17-EpDPE	.551*	.018	18	Pos	IP10	IFNa pathway
	10S,17S-DiHDoHE	.583*	.011	18	Pos		
CYP	5S,6S-DiHETE	.491*	.039	18	Pos	IL-10	Inflammasone/ Innate Pathway
	10S,17S-DiHDoHE	.503*	.033	18	Pos		
	12,13-DiHOME	-.578*	.012	18	Neg		
	5,6-EpETrE	.539*	.021	18	Pos	MIP-1beta	
	12,13-DiHODE	.675**	.002	18	Pos		
LOX	12-KETE	.489*	.039	18	Pos	IP10	IFNa pathway
	13-HODE	.497*	.036	18	Pos		
	LTB4	.505*	.032	18	Pos		
	8S,15S-DiHETE	.509*	.031	18	Pos		
	6-trans-LTB4	.517*	.028	18	Pos		
	9-HODE	.519*	.027	18	Pos		
	15-HETE	.542*	.020	18	Pos		
	9-HOTrE	.556*	.017	18	Pos		
	5S-HEPE	.624**	.006	18	Pos		
	9-HOTrE	.492*	.038	18	Pos	IL10	
	8S,15S-DiHETE	.558*	.016	18	Pos		
	12-HETE	.647**	.004	18	Pos	IL-1beta	
	9,10,13-TriHOME	.484*	.042	18	Pos	IL-8	
	9,12,13-TriHOME	.509*	.031	18	Pos		
	12S-HEPE	.523*	.026	18	Pos		
	12-HETE	.685**	.002	18	Pos		
	15S-HETrE	.471*	.048	18	Pos	MIP-1beta	Inflammasone/ Innate Pathway
	15-HETE	.491*	.038	18	Pos		
	9-HOTrE	.546*	.019	18	Pos		
	13-HODE	.555*	.017	18	Pos		
	9-HODE	.556*	.017	18	Pos		
	13-KODE	.560*	.016	18	Pos		
	9-KODE	.577*	.012	18	Pos		
	9,10,13-TriHOME	.687**	.002	18	Pos		
	9,12,13-TriHOME	.722**	.001	18	Pos		
	12S-HEPE	.786**	.000	18	Pos		
	12-HETE	.904**	.000	18	Pos		

Supplementary Figures

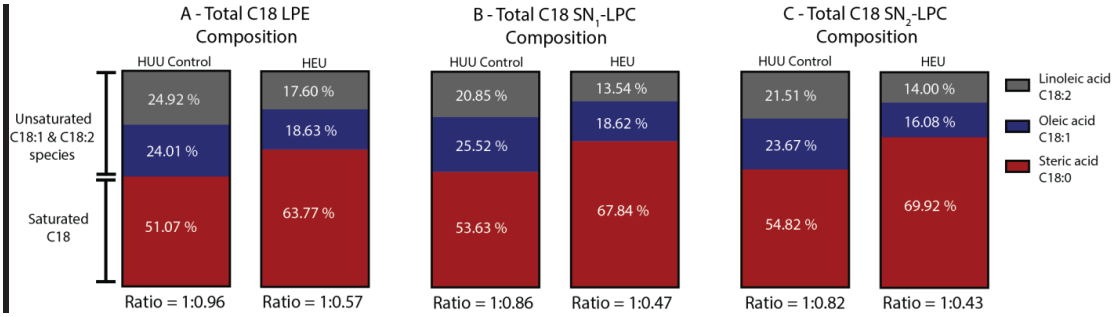

Figure S7.1: **Lysophospholipid C18 species composition:** Investigating the saturation vs. unsaturation ratio in the C18 LPE and $SN_{1/2}$-LPC species all showed the same trend. Due to the significant increases in stearic acid lysophopholipids and the downwards trend of the unsaturated C18 species the cART-exposed HEU infants shows an almost doubling in the ratio of stearic acid vs. oleic and linoleic acid species compared to HUU infants. Red, blue grey represent stearic acid (C18:0), oleic acid (C18:1) and linoleic acid (C18:2) respectively.

Supplementary Methods

1. Positive lipid profiling

Positive lipids were extracted with isopropyl alcohol (IPA). In short, 1000 µL IPA containing calibrant and internal standards both at C4 levels were added to 10 µL serum to precipitate proteins. After centrifugation (12.100 rpm, 10 mins, at RT) supernatant containing the lipids is transferred to vials for LC-MS analysis. In total 2.5 µL was injected for analysis.

1.1 Equipment

Chromatographic separation was achieved on an ACQUITY UPLC™ HSS T3 column (1.8 µm, 2.1 x 100mm) with a flow of 0.4 mL/min over a 16 min gradient. The lipid analysis is performed on a UPLC-ESI-Q-TOF (Agilent 6530, Jose, CA, USA) high resolution mass spectrometer using reference mass correction. Lipids were detected in full scan in the positive ion mode.

1.2 List of Detected Metabolites

Lipid Class	Lipidmaps	Metabolite species	Amount (n)
Cholesteryl ester (CE)	ST0102	C18:1; C18:2; C20:4; C22:6	4
Ceremides (Cer)	SP02	d18:0/24:0; d18:0/22:0; d18:1/22:0; d18:1/24:1; d18:1/24:0	5
Diacylglycerol (DG)	GL0201	C36:2; C36:3; C28:0	3
Lysophosphatidylcholine (LPC)	GP0105	C14:0; C16:0; C16:1; C18:0; C18:1; C18:2; C18:3; C19:0; C20:3; C20:4; C20:5; C22:6	12
Lysophosphatidylethanolamine (LPE)	GP0205	C18:0	1
Phosphatidylcholine (PC)	GP0101	C32:0; C32:1; C32:2; C34:1; C34:2; C34:3; C34:4; C36:1; C36:2; C36:3; C36:4; C36:5; C38:2; C38:3; C38:4; C38:5; C38:6; C38:7; C40:4; C40:5; C40:6; C40:7; C40:8	23
Phosphatidylethanolamine (PE)	GP0201	C30:0; C36:3; C36:4; C38:2; C38:4; C38:6	6
Plasmalogen Lysophosphatidylcholine (pLPC)	GP0106	C16:1; C18:1	2
Plasmalogen Phosphatidylcholine (pPC)	GP0102	C34:1; C34:2; C34:3; C36:4; C36:5; C36:6; C38:4; C38:5; C38:6; C38:7	10
Plasmalogen Phosphatidylethanolamine (pPE)	GP0202	C38:7	1
Sphingomyelins (SM)	SP0301	d18:1/14:0; d18:1/15:0; d18:1/16:0; d18:1/16:1; d18:1/18:0; d18:1/18:1; d18:1/18:2; d18:1/20:0; d18:1/20:1; d18:1/21:0; d18:1/22:0; d18:1/22:1; d18:1/23:0; d18:1/23:1; d18:1/24:0; d18:1/24:1; d18:1/24:2	17
Triglycerides (TG)	GL0301	C48:0; C48:1; C48:2; C48:3; C48:4; C50:0; C50:1; C50:2; C50:3; C50:4; C51:1; C51:2; C51:3; C52:0; C52:1; C52:2; C52:3; C52:4; C52:5; C54:1; C54:2; C54:3; C54:4; C54:5; C54:6; C54:7; C55:2; C55:3; C56:3; C56:7; C56:8; C58:2; C58:5; C58:6; C58:8; C58:10	35

2. Polar negative lipid profiling

Polar lipid extraction is performed by methanol extraction. Briefly, 440 µL methanol containing internal standard is added to 20 µL serum. After centrifugation, the protein is precipitated and the lipid containing supernatant is transferred to clean Eppendorf tubes and the solvent is evaporated using a Speedvac. The dried lipids were reconstituted in 145 µL isopropanol, 0.1% formic acid and transferred to autosampler vials. In total 8 µL was injected for analysis.

2.1 Equipment

Chromatographic separation was achieved on an ACQUITY UPLC™ HSS T3 column with a flow of 0.4 ml/min over 15 min gradient. Free fatty acids and lyso-phospholipid content is analyzed with a UPLC-ESI-Q-TOF (Agilent 6530, Jose, CA, USA) high resolution mass spectrometer using reference mass correction. Polar lipids were detected in full scan in the negative ion mode.

2.2 List of Detected Metabolites

Lipid Class	Lipidmaps	Metabolite species	Amount (n)
Free fatty acids (FA)	FA01	C14:0; C17:1; C18:1; C18:2; C18:3-(w3w6); C20:1; C20:2; C20:3-(w9); C20:3-(w3w6); C20:4-(w6); C20:5-(w3); C22:0; C22:2; C22:3; C22:4; C22:5-(w3); C22:5-(w6); C22:6; C24:1; C24:2	21
Lysophosphatidylcholine (LPC)	GP0105	*sn1:* C14:0; C15:0; C16:0; C16:1; C18:0; C18:1; C18:2; C20:1; C20:2; C20:3-(w9); C20:3-(w3w6); C20:4; C20:5; C22:4; C22:5-(w3); C22:5-(w6); C22:6 *sn2:* C14:0; C16:0; C16:1; C18:0; C18:1; C18:2; C20:3-(w3w6); C20:4; C20:5; C22:6	28
Lysophosphatidylethanolamine (LPE)	GP0205	C16:0; C18:0; C18:1; C18:2; C20:3-(w3w6); C20:4; 22:5-(w3); 22:5-(w6); C22:6	9
Plasmalogen Lysophosphatidylcholine (pLPC)	GP0106	C16:0; C18:0; C18:1; C18:2	4

3. Oxylipin profiling

The oxylipin platform covers classical and non-classical eicosanoids from different poly unsaturated fatty acids (PUFA), including n-6 and n-3 PUFAs such as linoleic acid and arachidonic acid (both n-6) and eicosapentaenoic acid (EPA) and docosahexaenoic acid (DHA) (both n-3). 250 µL of each plasma sample were spiked with antioxidants and internal standard mix (Table 8), diluted and add to the SPE cartridge using a hydrophilic-lipophilic balance (HLB) (Oasis, Waters). Oxylipins were eluted with methanol and ethyl acetate. To concentrate, the eluate was gently dried under nitrogen stream and reconstituted in 50 µL of injection solvent (acetonitrile and methanol,1:1 v/v). In total 5 µL was injected for analysis.

3.1 Equipment

The HPLC was coupled to electrospray ionization on a triple quadrupole mass spectrometer (Agilent 6460, San Jose, CA, USA). Separation was done by HPLC (Agilent 1260, San Jose, CA, USA) using an Ascentis® Express column (2.1x150 mm, 2.7 µm particles; Supelco, Bellefonte, PA, USA) with 0.35 mL flow during 28 min gradient. Oxylipins were detected in negative ion mode using dynamic Multiple Reaction Monitoring (MRM).

3.2 List of Detected Metabolites

Metabolite	Systematic Name	Chemical formula	Lipid maps ID	Inchy-Key
10-HDoHE	(+/-)-10-hydroxy-4Z,7Z,11E,13Z,16Z,19Z-docosahexaenoic acid	C22H32O3	LMFA04000027	DDCYKEYDTGCKAS-SKSHMZPZSA-N
10S,17S-DiHDoHE	10(S),17(S)-dihydroxy-4Z,7Z,11E,13Z,15E,19Z-docosahexaenoic acid	C22H32O4	LMFA04000047	CRDZYJSQHCXHEG-XLBFCUQGSA-N
11,12-DiHETrE	(±)11,12-dihydroxy-5Z,8Z,14Z-eicosatrienoic acid	C20H34O4	LMFA03050008	LRPPQRCHCPFBPE-LZXKBWHHSA-N
11,12-EpETrE	(±)11(12)-epoxy-5Z,8Z,14Z-eicosatrienoic acid	C20H32O3	LMFA03080014	DXOYQVHGIODESM-LZXKBWHHSA-N
11beta-13,14-dihydro-15-keto-PGF2a	9S,11R-dihydroxy-15-oxo-prost-5Z-en-1-oic acid	C20H34O5	LMFA03010203	VKTIONYPMSCHQI-KGILNJEGSA-N
11beta-PGE2	9-oxo-11S,15S-dihydroxy-5Z,13E-prostadienoic acid	C20H32O5	LMFA03010060	XEYBRNLFEZDVAW-YUOXZBOXSA-N
11-HDoHE	(+/-)-11-hydroxy-4Z,7Z,9E,13Z,16Z,19Z-docosahexaenoic acid	C22H32O3	LMFA04000028	LTERDCBCHFKFRI-BGKMTWLOSA-N
11-HETE	11R-hydroxy-5Z,8Z,12E,14Z-eicosatetraenoic acid	C20H32O3	LMFA03060028	GCZRCCHPLVMMJE-WXMXURGXSA-N
12,13-DiHODE	(+/-)-12,13-dihydroxy-9Z,15Z-octadecadienoic acid	C18H32O4	LMFA02000046	RGRKFKRAFZJQMS-OOHFSOINSA-N
12,13-DiHOME	12,13-dihydroxy-9Z-octadecenoic acid	C18H34O4	LMFA01050351	CQSLTKIXAJTQGA-GJGKEFFFSA-N
12,13-EpOME	(+/-)-12(13)-epoxy-9Z-octadecenoic acid	C18H32O3	LMFA02000038	CCPPLIJZDQAOHD-FLIBITNWSA-N
12-HETE	12-hydroxy-5Z,8Z,10E,14Z-eicosatetraenoic acid	C20H32O3	LMFA03060088	ZNHVWPKMFKADKW-VXBMJZGYSA-N
12-KETE	12-oxo-5Z,8Z,10E,14Z-eicosatetraenoic acid	C20H30O3	LMFA03060019	GURBRQGDZZKITB-VXBMJZGYSA-N
12S-HEPE	12S-hydroxy-5Z,8Z,10E,14Z,17Z-eicosapentaenoic acid	C20H30O3	LMFA03070008	MCRJLMXYVFDXLS-UOLHMMFFSA-N
12S-HHTrE	12S-hydroxy-5Z,8E,10E-heptadecatrienoic acid	C17H28O3	LMFA03050002	KUKJHGXXZWHSBG-WBGSEQOASA-N
12S-HpETE	12S-hydroperoxy-5Z,8Z,10E,14Z-eicosatetraenoic acid	C20H32O4	LMFA03060013	ZIOZYRSDNLNNNJ-VXBMJZGYSA-N
13,14-dihydro-15-keto-PGD2	11,15-dioxo-9S-hydroxy-5Z-prostenoic acid	C20H32O5	LMFA03010022	VSRXYLYXIXYEST-KZTWKYQFSA-N
13,14-dihydro-15-keto-PGE2	9,15-dioxo-11R-hydroxy-5Z-prostenoic acid	C20H32O5	LMFA03010031	CUJMXIQZWPZMNQ-XYYGWQPLSA-N

13,14-dihydro-15-keto-PGF2a	9S,11S-dihydroxy-15-oxo-5Z-prostenoic acid	C20H34O5	LMFA03010027	VKTIONYPMSCHQI-XAGFEHLVSA-N
13,14-dihydro-PGF2a	9S,11R,15S-trihydroxy-5Z-prostenoic acid	C20H36O5	LMFA03010079	LLQBSJQTCKVWTD-QPJJXVBHSA-N
13-HDoHE	(+/-)-13-hydroxy-4Z,7Z,10Z,14E,16Z,19Z-docosahexaenoic acid	C22H32O3	LMFA04000029	SEVOKGDVLLIUMT-SKSHMZPZSA-N
13-HODE	13S-hydroxy-9Z,11E-octadecadienoic acid	C18H32O3	LMFA02000154	HNICUWMFWZBIFP-BSZOFBHHSA-N
13-HpODE	(±)13-hydroperoxy-9Z,11E-octadecadienoic acid	C18H32O4	LMFA02000034	JDSRHVWSAMTSSN-BSZOFBHHSA-N
13-KODE	13-keto-9Z,11E-octadecadienoic acid	C18H30O3	LMFA02000016	JHXAZBBVQSRKJR-BSZOFBHHSA-N
14,15-DiHETrE	14,15-dihydroxy-5Z,8Z,11Z-eicosatrienoic acid	C20H34O4	LMFA03050010	SYAWGTIVOGUZMM-ILYOTBPNSA-N
14,15-DiHETrE	(±)14,15-dihydroxy-5Z,8Z,11Z-eicosatrienoic acid	C20H34O4	LMFA03050010	SYAWGTIVOGUZMM-KZTFMOQPSA-N
14,15-EpETrE	(±)14(15)-epoxy-5Z,8Z,11Z-eicosatrienoic acid	C20H32O3	LMFA03080013	JBSCUHKPLGKXKH-KZTFMOQPSA-N
14-HDoHE	(+/-)-14-hydroxy-4Z,7Z,10Z,12E,16Z,19Z-docosahexaenoic acid	C22H32O3	LMFA04000030	ZNEBXONKCYFJAF-BGKMTWLOSA-N
15-deoxy-delta-12,14-PGD2	9S-hydroxy-11-oxo-5Z,12E,14E-prostatrienoic acid	C20H30O4	LMFA03010051	QUGBPWLPAUHDTI-PLGLXCLHSA-N
15-HETE	15S-hydroxy-5Z,8Z,11Z,13E-eicosatetraenoic acid	C20H32O3	LMFA03060001	JSFATNQSLKRBCI-VAEKSGALSA-N
15S-HEPE	15S-hydroxy-5Z,8Z,11Z,13E,17Z-eicosapentaenoic acid	C20H30O3	LMFA03070009	WLKCSMCLEKGITB-DBVSHIMFSA-N
15-keto-PGF2a	9S,11R-dihydroxy-15-oxo-5Z,13E-prostadienoic acid	C20H32O5	LMFA03010026	LOLJEILMPWPILA-AMFHKTBMSA-N
15S-HETrE	15S-hydroxy-8Z,11Z,13E-eicosatrienoic acid	C20H34O3	LMFA03050007	IUKXMNDGTWTNTP-OAHXIXLCSA-N
16,17-EpDPE	(±)16(17)-epoxy-4Z,7Z,10Z,13Z,19Z-docosapentaenoic acid	C22H32O3	LMFA04000037	BCTXZWCPBLWCRV-QCAYAECISA-N
16-HDoHE	(±)16-hydroxy-4Z,7Z,10Z,13Z,17E,19Z-docosahexaenoic acid	C22H32O3	LMFA04000031	CSXQXWHAGLIFIH-VUARBJEWSA-N
17,18-DiHETE	(+/-)-17,18-dihydroxy-5Z,8Z,11Z,14Z-eicosatetraenoic acid	C20H32O4	LMFA03060078	XYDVGNAQQFWZEF-JPURVOHMSA-N
17-HDoHE	(±)17-hydroxy-4Z,7Z,10Z,13Z,15E,19Z-docosahexaenoic acid	C22H32O3	LMFA04000032	SWTYBBUBEPPYCX-VIIQGJSXSA-N
18-HEPE	(±)-18-hydroxy-5Z,8Z,11Z,14Z,16E-eicosapentaenoic acid	C20H30O3	LMFA03070033	LRWYBGFSVUBWMO-UXNZXXPISA-N
19,20-DiHDPA	(±)19,20-dihydroxy-4Z,7Z,10Z,13Z,16Z-docosapentaenoic acid	C22H34O4	LMFA04000043	FFXKPSNQCPNORO-MBYQGORISA-N
19,20-EpDPE	(+/-)-19(20)-epoxy-4Z,7Z,10Z,13Z,16Z-docosapentaenoic acid	C22H32O3	LMFA04000038	OSXOPUBJJDUAOJ-MBYQGORISA-N
20-carboxy-LTB4	5S,12R-dihydroxy-6Z,8E,10E,14Z-eicosatetraene-1,20-dioic acid	C20H30O6	LMFA03020016	SXWGPVJGNOLNHT-VFLUTPEKSA-N

20-HDoHE	(+/-)-20-hydroxy-4Z,7Z,10Z,13Z,16Z,18E-docosahexaenoic acid	C22H32O3	LMFA04000033	YUZXOJOCNGKDNI-LFVREGEGSA-N
20-hydroxy-LTB4	5S,12R,20-trihydroxy-6Z,8E,10E,14Z-eicosatetraenoic acid	C20H32O5	LMFA03020018	PTJFJXLGRSTECQ-PSPARDEHSA-N
20-hydroxy-PGE2	9-oxo-11R,15S,20-trihydroxy-5Z,13E-prostadienoic acid	C20H32O6	LMFA03010014	AZIGEYVZEVXWAD-NZGURKHLSA-N
4-HDoHE	(±)4-hydroxy-5E,7Z,10Z,13Z,16Z,19Z-docosahexaenoic acid	C22H32O3	LMFA04000024	IFRKCNPQVIJFAQ-PQVBWYSWSA-N
5,6-DiHETrE	5S,6S-dihydroxy-7E,9E,11Z,14Z-eicosatetraenoic acid	C20H32O4	LMFA03060018	UVZBUUTTYHTDRR-WAQVJNLQSA-N
5,6-EpETrE	(±)5(6)-epoxy-8Z,11Z,14Z-eicosatrienoic acid	C20H32O3	LMFA03080017	VBQNSZQZRAGRIX-GSKBNKFLSA-N
5-HETE	5S-hydroxy-6E,8Z,11Z,14Z-eicosatetraenoic acid	C20H32O3	LMFA03060002	KGIJOOYOSFUGPC-JGKLHWIESA-N
5-HETrE	5S-hydroxy-6E,8Z,11Z-eicosatrienoic acid	C20H34O3	LMFA03050005	LSADDRSUZRRBAN-FDSUASFTSA-N
5-iPF2a-VI	5,9S,11R-trihydroxy-6E,14Z-prostadienoic acid-cyclo[8S,12R]	C20H34O5	LMFA03110011	RZCPXIZGLPAGEV-SUHLLOIRSA-N
5-KETE	5-oxo-6E,8Z,11Z,14Z-eicosatetraenoic acid	C20H30O3	LMFA03060011	MEASLHGILYBXFO-XTDASVJISA-N
5S,14R-Lipoxin B4	5S,14R,15S-trihydroxy-6E,8Z,10E,12E-eicosatetraenoic acid	C20H32O5	LMFA03040002	UXVRTOKOJOMENI-WLPVFMORSA-N
5S,15S-DiHETE	5S,15S-dihydroxy-6E,8Z,10Z,13E-eicosatetraenoic acid	C20H32O4	LMFA03060010	UXGXCGPWGSUMNI-BVHTXILBSA-N
5S,6R-LipoxinA4	5S,6R,15S-trihydroxy-7E,9E,11Z,13E-eicosatetraenoic acid	C20H32O5	LMFA03040001	IXAQOQZEOGMIQS-SSQFXEBMSA-N
5S,6S-DiHETE	5S,6S-dihydroxy-7E,9E,11Z,14Z-eicosatetraenoic acid	C20H32O4	LMFA03060018	UVZBUUTTYHTDRR-WAQVJNLQSA-N
5S,6S-Lipoxin A4	5S,6R,15S-trihydroxy-7E,9E,11Z,13E-eicosatetraenoic acid	C20H32O5	LMFA03040001	IXAQOQZEOGMIQS-SSQFXEBMSA-N
5S-HEPE	5S-hydroxy-6E,8Z,11Z,14Z,17Z-eicosapentaenoic acid	C20H30O3	LMFA03070010	FTAGQROYQYQRHF-GHWNLOBHSA-N
6-keto-PGF1a	6-oxo-9S,11R,15S-trihydroxy-13E-prostenoic acid	C20H34O6	LMFA03010001	KFGOFTHODYBSGM-ZUNNJUQCSA-N
6-trans-LTB4	5S,12R-dihydroxy-6E,8E,10E,14Z-eicosatetraenoic acid	C20H32O4	LMFA03020013	VNYSSYRCGWBHLG-UKNWISKWSA-N
7-HDoHE	(±)7-hydroxy-4Z,8E,10Z,13Z,16Z,19Z-docosahexaenoic acid	C22H32O3	LMFA04000025	OZXAIGIRPOOJTI-XJAVJPOHSA-N
8,9-DiHETrE	8,9-dihydroxy-5Z,11Z,14Z-eicosatrienoic acid	C20H34O4	LMFA03050006	DCJBINATHQHPKO-TYAUOURKSA-N
8,9-EpETrE	(±)8(9)-epoxy-5Z,11Z,14Z-eicosatrienoic acid	C20H32O3	LMFA03080019	DBWQSCSXHFNTMO-ZZMPYBMWSA-N
8_HDoHE	(±)8-hydroxy-4Z,6E,10Z,13Z,16Z,19Z-docosahexaenoic acid	C22H32O3	LMFA04000026	ZHBVYDMSPDDAKE-VTIZNUJUSA-N
8-HETE	(±)8-hydroxy-5Z,9E,11Z,14Z-eicosatetraenoic acid	C20H32O3	LMFA03060086	NLUNAYAEIJYXRB-HEJOTXCHSA-N

8-HETrE	8S-hydroxy-9E,11Z,14Z-eicosatrienoic acid	C20H34O3	LMFA03050011	SKIQVURLERJJCK-RDCCVJQZSA-N
8-iso-PGF2a	9S,11R,15S-trihydroxy-5Z,13E-prostadienoic acid-cyclo[8S,12R]	C20H34O5	LMFA03110001	PXGPLTODNUVGFL-NAPLMKITSA-N
8S,15S-DiHETE	8S,15S-dihydroxy-5Z,9E,11Z,13E-eicosatetraenoic acid	C20H32O4	LMFA03060050	NNPWRKSGORGTIM-HCCKYKKOSA-N
9,10,13-TriHOME	E)-9,10,13-Trihydroxy-11-octadecenoic acid	C18H34O5	LMFA02000168	NTVFQBIHLSPEGQ-BUHFOSPRSA-N
9,10-DiHOME	9,10-dihydroxy-12Z-octadecenoic acid	C18H34O4	LMFA02000229	XEBKSQSGNGRGDW-CJWPDFJNSA-N
9,10-EpOME	(+/-)-9(10)-epoxy-12Z-octadecenoic acid	C18H32O3	LMFA02000037	FBUKMFOXMZRGRB-XKJZPFPASA-N
9,12,13-TriHOME	9S,12S,13S-trihydroxy-10E-octadecenoic acid	C18H34O5	LMFA02000014	MDIUMSLCYIJBQC-MVFSOIOZSA-N
9-HEPE	(±)-9-hydroxy-5Z,7E,11Z,14Z,17Z-eicosapentaenoic acid	C20H30O3	LMFA03070029	OXOPDAZWPWFJEW-IMCWFPBLSA-N
9-HETE	(±)-9-hydroxy-5Z,7E,11Z,14Z-eicosatetraenoic acid	C20H32O3	LMFA03060089	KATOYYZUTNAWSA-OIZRIKEUSA-N
9-HODE	(±)-9-hydroxy-10E,12Z-octadecadienoic acid	C18H32O3	LMFA02000151	NPDSHTNEKLQQIJ-ZJHFMPGASA-N
9-HOTrE	9S-hydroxy-10E,12Z,15Z-octadecatrienoic acid	C18H30O3	LMFA02000024	RIGGEAZDTKMXSI-MEBVTJQTSA-N
9-KODE	9-oxo-10E,12Z-octadecadienoic acid	C18H30O3	LMFA02000274	LUZSWWYKKLTDHU-ZJHFMPGASA-N
bicyclo-PGE2	9,15-dioxo-5Z-prostaenoic acid-cyclo[11S,16]	C20H30O4	LMFA03010034	CGCZPIJMGKLVTQ-PAJBVNRRSA-N
d12-PGJ2	11-oxo-15S-hydroxy-prosta-5Z,9,12E-trien-1-oic acid	C20H30O4	LMFA03010020	TUXFWOHFPFBNEJ-GJGHEGAFSA-N
LTB4	5S,12R-dihydroxy-6Z,8E,10E,14Z-eicosatetraenoic acid	C20H32O4	LMFA03020001	VNYSSYRCGWBHLG-AMOLWHMGSA-N
PGD1	9S,15S-dihydroxy-11-oxo-13E-prostaenoic acid	C20H34O5	LMFA03010049	CIMMACURCPXICP-PNQRDDRVSA-N
PGE2	9-oxo-11R,15S-dihydroxy-5Z,13E-prostadienoic acid; Prostin E2	C20H32O5	LMFA03010003	XEYBRNLFEZDVAW-ARSRFYASSA-N
PGF2a	9S,11R,15S-trihydroxy-5Z,13E-prostadienoic acid	C20H34O5	LMFA03010002	PXGPLTODNUVGFL-YNNPMVKQSA-N
PGJ2	11-oxo-15S-hydroxy-prosta-5Z,9,13E-trien-1-oic acid	C20H30O4	LMFA03010019	UQOQENZZLBSFKO-POPPZSFYSA-N
TXB2	9S,11,15S-trihydroxy-thromboxa-5Z,13E-dien-1-oic acid	C20H34O6	LMFA03030002	XNRNNGPBEPRNAR-JQBLCGNGSA-N